Development of nanoparticle catalysts and total internal reflection (TIR) Raman spectroscopy for improved understanding of heterogeneous catalysis

BINGHAM, LAURA,MARIA

Chapter 1. Introduction

1.1. An introduction to heterogeneous catalysis, and the need for surface sensitive characterisation, and model catalysts

Formally, a catalyst is defined as a species which increases the rate of a chemical reaction. This takes place without the catalyst itself being consumed.[1] This is achieved by providing an alternate reaction route, with a lower activation energy than for the uncatalysed one (Figure 1.1 A). For heterogeneous catalysts specifically the general reaction path is given in Figure 1.1 B. First adsorption onto the catalyst surface occurs (usually an exothermic process), this is followed by reaction of the adsorbed species, perhaps *via* intermediate formation, followed by formation of the overall transition state (in which bond breaking and forming is seen). Finally desorption of the adsorbed product is seen in a typically endothermic process. Catalysts allow manufacturers of chemical products to reduce the energy input required. They can also allow the reaction to be directed along a specific pathway, to give products that cannot usually be produced. Catalysts are therefore of significant industrial importance, and are used within the production of the majority of consumer goods. Examples include the Haber process, in which iron is used to catalyse the conversion of nitrogen and hydrogen to ammonia. This process is used in the production of fertiliser.[2] Another such example is the use of catalysts for crude oil refining, in the production of automotive fuels. Catalysts are used both in the refining and final emission control stages.[3] Therefore the study of catalysis is not only potentially important for commercial reasons, but also has wide-ranging impact across many application areas.

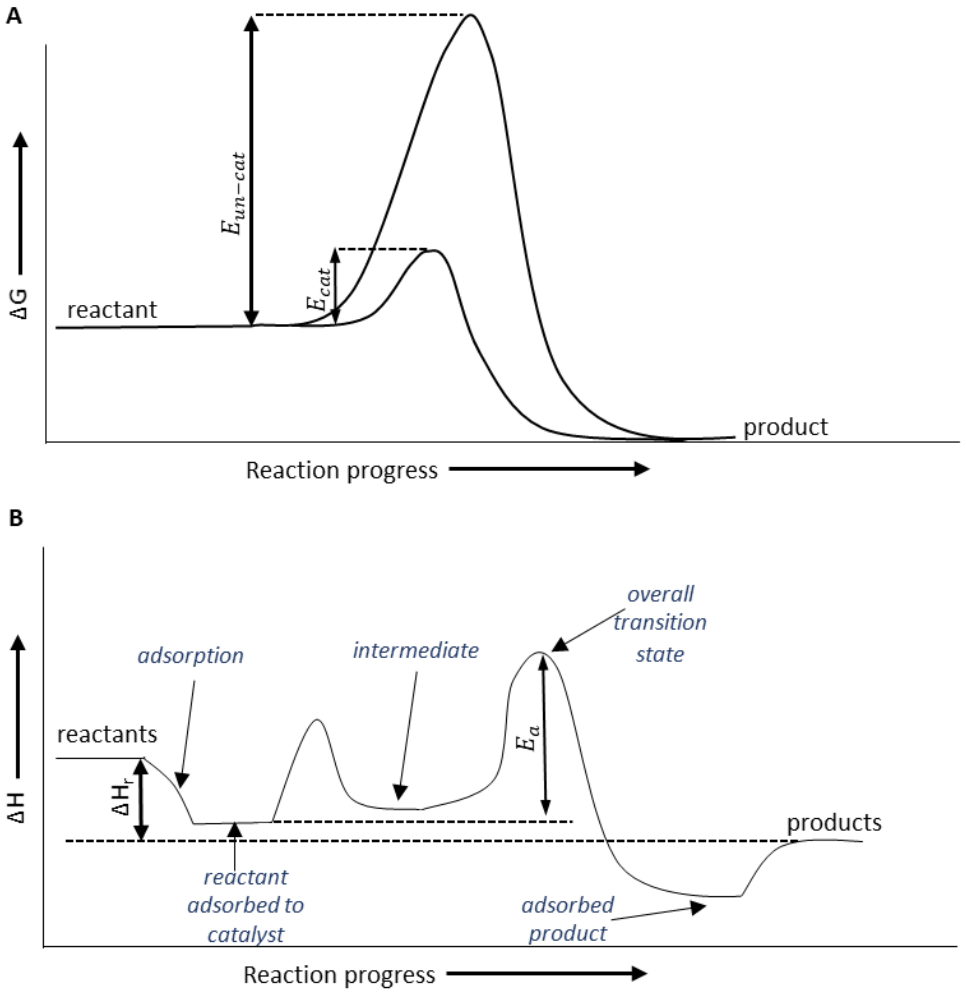

Figure 1.1. Schematic of the A) generic reaction path (energy vs. reaction progress) for catalysed and un-catalysed reactions, where E_{cat} and E_{uncat} are the activation energies for the catalysed and uncatalysed reaction respectively, and B) reaction path for heterogeneous catalytic process, where E_a is the activation energy for the overall process.

Catalysis is an umbrella term that can be split broadly into three fields: homogeneous, enzymatic, and heterogeneous. In homogeneous catalysis, the catalyst is in the same phase as the reactants and products, the liquid phase is one of the most common.[4] Enzymes are responsible for catalysis in biological systems were their nature is somewhat intermediate of heterogeneous and homogeneous catalysts.[2] In heterogeneous catalysis, the catalyst and reactants are in different phases, *i.e*. solid catalysts with gas and/or liquid reagents.[5] Around 90% of the catalysts used in petrochemical-based industrial processes are heterogeneous. In addition, many processes in the energy, automotive, and fine chemical sectors are mediated primarily by heterogeneous catalysts.[6,7] There are various reasons for the widespread use of heterogeneous catalysis over homogeneous systems in industry, which include ease of separation, catalyst recyclability, as well as continuous plant use over that of a batch process.[2] However, one major disadvantage of heterogeneous catalysis, and in particular

solid state catalysts, is that the reaction mechanisms are relatively less well understood than their homogeneous counterparts. This is particularly true in terms of understanding of these processes under realistic operating pressures and temperatures.[6] The deduction of mechanisms in solid-state catalysis, is made somewhat more complicated by interfacial properties such as surface diffusion and adsorption, which can impact upon the reaction rate. Such properties are challenging both to measure experimentally, and to separate from the surface chemistry. For example, it is relatively simple to study the disappearance of reactant, and appearance of product. It is, however, more difficult to measure other properties such as the rates and energetics of adsorption, the structure of the active surface, or the nature of reactive intermediates.[5] In contrast, solution-phase catalysts may be monitored using dynamic techniques, such as nuclear magnetic resonance (NMR) spectroscopy. Additionally, reaction mechanisms in homogeneous catalysis involve intermediates that can be isolated and characterised using techniques such as NMR spectroscopy and X-ray diffraction (XRD). For solid heterogeneous catalysts, reaction chemistry occurs at the surface. If we wish to understand the reaction kinetics and the overall mechanism, then we must probe at the catalyst surface. Surface-specific analytical techniques, such as X-ray photoelectron spectroscopy (XPS) and low-energy ion scattering (LEIS), may be used in combination to gain information on the surface structure of the catalyst and allow mechanistic understanding to be ascertained. If such techniques take place as the reaction occurs (under realistic operating conditions), then more relevant and realistic data might be gained. This has given rise to the use of surface sensitive *in situ* and *operando* characterisation techniques (see Chapter 1, Sections 1.2, and 1.3 for details).[6,8]

Also of importance in interrogating catalyst properties, is developing a suitable model catalyst. The complexity of an industrial catalyst can complicate spectroscopic and kinetic interpretation. This is due to the catalyst having a varying range of properties including particle size, shape and additives. In contrast a model catalyst, a deliberately simplified catalyst material, can allow for the spectroscopy and kinetics to be measured on a well-defined system. Complexity of different additives can then be added in individual steps. In its simplest form such a model catalyst might be a metal single crystal, which have been used to study an extensive number of metal-catalysed surface processes.[9] Equally, more complex catalyst models may be needed to probe some phenomena that occur in catalysis, such as metal-support interactions or particle size effects.[10] The single crystal approach is particularly useful in cases where the complexity of the catalytic system would otherwise be very difficult

or impossible to study. This allows for better understanding and expansion of the results obtained to systems closer to those present in practical catalysts.[8]

The development of well-defined model catalysts, and the subsequent *in situ* study at the catalyst surface, during catalytically operational conditions, is the long term aim of this work. This takes place with the novel use of a total internal reflection (TIR) Raman spectroscopic technique as explored in Section 1.4.

1.1.1. Why study heterogeneous catalysts *in situ*?

Work in the field of catalysis initially focused upon monitoring of the reagent and the product, but this is often disparagingly viewed as "magic box" science referring to the unknown that exists between these two stages.[11] It has been previously noted within this report that, for heterogeneous catalysts, such an approach is not sufficient to give detailed mechanistic understanding (*i.e.* reaction kinetics, reaction intermediates). In particular such an approach lacks any focus upon understanding interfacial properties such as adsorption. Much work has been done, to try to understand such interfacial properties. One prominent approach is the use of single crystals under ultra-high vacuum (UHV). Such work uses a single crystal to model the catalyst system, and a UHV analysis with a high pressure chamber or cell allowing transfer between reactive gases and vacuum for analysis without exposure to air. This allows the surface chemistry to be studied after exposure to high pressures and temperatures,[11] examples studied include ammonia synthesis,[12–14] and Fischer-Tropsch.[15–17] Results have shown good correlation between the single crystal UHV and real catalyst systems.[18,19,20] Many important findings have been made including the identification of the importance of defect sites,[21] and the verification of the classification of reactions as structure sensitive and insensitive.[22,23]

However, despite the correlation seen between the results for the two there was some question as to how well these systems modelled real catalysts under typical industrial pressures (1-100 atm). Differences in actual catalyst behaviour due to differences in the gas pressures used is known as the pressure gap. The pressure gap takes into account differences in surface structure and chemistry between catalysts in real and UHV conditions.[16] Underpinning concerns about the pressure gap was the belief that a material's structure and composition might change upon experience of real world catalyst conditions. At the time *post-mortem* analysis of used catalysts had been employed to examine this theory, but the validity of results was debated, since the catalysts' material properties might be reversible and change upon completion of the reaction and removal from the reactor.[17] Publications

such as that by Rupprechter and Weilach began to explore the difference between single crystal and high vacuum techniques, with those done at more realistic conditions.[24–26]

Under high pressure conditions Zaera *et al.* states that for a variety of reactions the catalyst surface might be covered in strongly bonded intermediates.[27] Such intermediates are typically also observed using UHV techniques, so in this case at least some agreement between high pressure, real world, and vacuum systems was seen. Another example in which single crystal UHV studies successfully reproduced data for real catalysts is the methanation of hydrogen and carbon monoxide.[28]

Despite some agreement being seen overall these considerations led to significant questions being posed about the validity of work conducted with these UHV single crystal systems. This led to the view that *in situ* surface characterisation techniques (*i.e.* ones that can be performed under more industrially applicable conditions) would be needed to provide a credible answer as to the true behaviour of the catalyst. This has given rise to a rapid expansion in the use of *in situ* surface spectroscopy.

1.2. *In situ* techniques for studying heterogeneous catalysts

Many techniques are available for *in situ* analysis of heterogeneous catalysts. For example the review by Zhang *et al.* details such techniques applicable to nanoparticle catalysis.[29] The complementary use of such techniques is commonly used to build up information about the catalyst surface.[30–32] It is our intention to use TIR Raman spectroscopy (Section 1.4) in such a manner. Therefore, the evaluation of the capabilities and limitations of other such techniques was required to illustrate how TIR Raman fits within this field. Such evaluation is given within the sections below.

1.2.1. Sum frequency generation (SFG)

Sum frequency generation (SFG) is a technique commonly used to study heterogeneous catalytic reactions. SFG can be used *in situ* as the reaction occurs and has allowed elucidation of much information about the nature of surface intermediates. The technique has found much use for high pressure, single crystal work. Its advantages include, that it is non-destructive, has surface sensitivity, has good spectral resolution, and the IR and visible light used pass through many gas atmospheres.[33] One challenge faced by SFG is that it occurs at an interface, but the location and extent of this interface is not always clear due to limitations in the fundamental theoretical understanding. Furthermore SFG is a function of both orientation and concentration effects, so the data SFG generates can be harder to interpret.

The particular suitability of such a technique to the study of heterogeneous catalysis is exemplified using the short case study given below.

Case study

Yang, and Somorjai *et al.* used SFG spectroscopy to study adsorption and surface reaction.[34] Specifically, they monitored adsorption geometries and surface reactions for various C_6 hydrocarbons on a platinum(III) single crystal. This was conducted both with and without an excess of hydrogen. Such work had application into many fields including adhesion, lubrication, and molecular surface dynamics, as it could help provide information on two-dimensional ordering and dynamic processes for large organics on surfaces. However, the intended goal of this work was the utilisation of SFG to study naphtha reforming, which is important for the synthesis of high octane fuels and so to heterogeneous catalysis.

The motivation to use SFG for such analysis came from the greater pressure ranges available as compared to other analytical techniques. Techniques such as low-energy electron diffraction (LEED),[9,35] and single crystal temperature programmed desorption (TPD),[36,37] which have been widely used for such studies, only operate under low pressure conditions ($<10^{-6}$ Torr). At such pressures only strongly adsorbed species are present, weakly bonded species desorb quickly. The naphtha reforming process, however, is conducted under high pressures. Weakly bonded species could play crucial roles in the mechanism, and could represent key reaction intermediates. SFG was therefore used as it is a surface sensitive technique which can operate at the near ambient pressures required (1.5 Torr of C_6 alkane, 15 Torr of hydrogen).

The authors chose to examine the following compounds: *n*-hexane, 2-methylpentane, 3-methylpentane, and 1-hexene, at various temperatures both with and without an excess of hydrogen. A temperature dependent series, in which temperature was steadily increased from 296 to 453 K was recorded. This allowed the species on the surface to be traced under the varying conditions. The authors normalised the SFG signal obtained to the intensity of the incident infrared beam on the surface. This was necessary as gas molecules in a high pressure cell can absorb some of the incident beam. The SFG bands obtained were assigned to the various stretching modes present in the molecules, and from this the molecule present and in some cases its orientation was determined.

Figure 1.2 schematically depicts the catalytic transformations seen. Using SFG the authors determined that, at 296 K and in the absence of an excess of hydrogen, *n*-hexane and 3-methylpentane readily dehydrogenated to give a π-allyl c-C_6H_9 and a metallocyclohexane

(Figure 1.2, A)i) and A)ii)). Furthermore at 453 K the π-allyl c-C_6H_9 undergoes irreversible dehydrogenation to yield a hexylidyne as well as the unreacted metallocycle hexane. The π-allyl c-C_6H_9 was assigned as a reactive intermediate for *n*-hexane as it undergoes dehydrocyclisation to form hexylidyne. It was, therefore, suggested that benzene formation, from *n*-hexane on platinum(III), goes *via* a 1-6 ring closure rather than a 5 member cyclic intermediate, whereas under conditions providing an excess of hydrogen, at 296 K, *n*-hexane and 3-methylpentane are inactive on platinum(III) (Figure 1.2, B)i) and B)ii)). Whilst, under these conditions, 2-methyl pentane and 1-hexene were dehydrogenated to yield metallocyclobutane and hexylidyne (Figure 1.2, C)i) and C)ii)). An increase of the reaction temperature to 453 K gave partial dehydrogenation of *n*-hexane and 3-methylpentane to yield a hexylidyne or metallocyclic species.

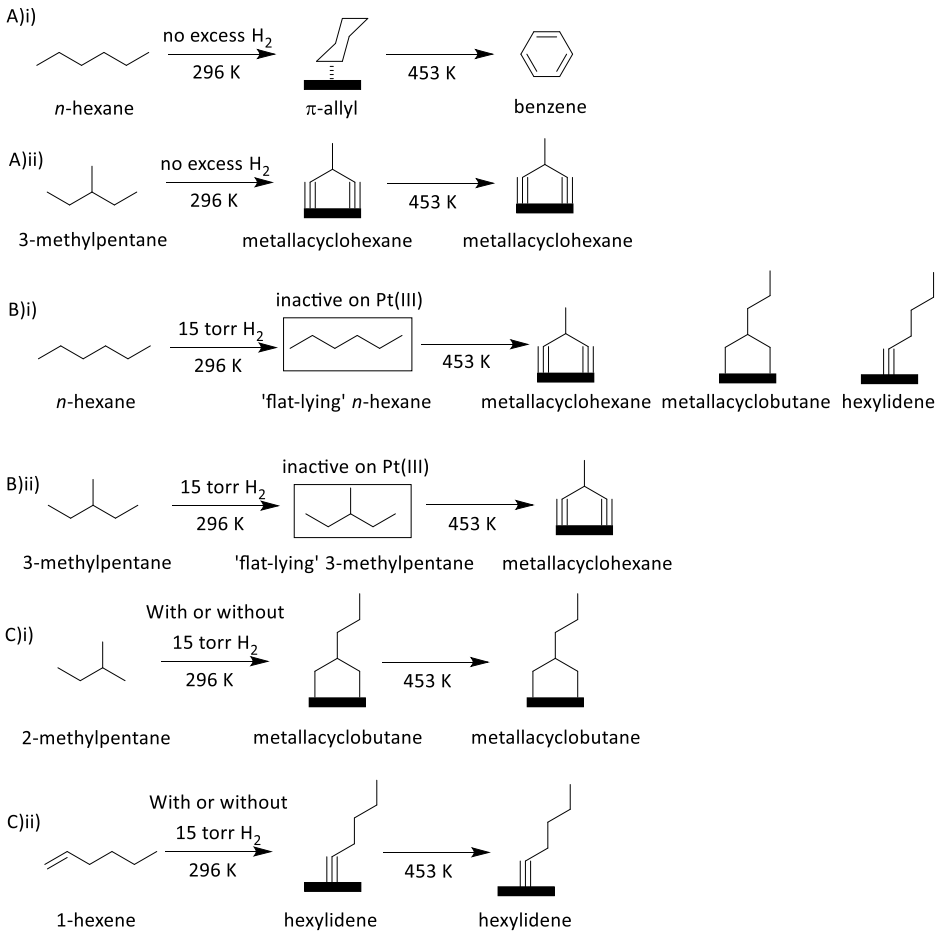

Figure 1.2. Schematic for catalytic transformations that occur under differing temperatures and hydrogen pressures, adapted from Yang and Somorjai.[34]

This example elucidates one possible use of SFG as a surface sensitive technique to probe reactive surface intermediates. Through determination of the nature and orientation of the

species present at the catalyst surface greater mechanistic insight was gained. Furthermore this was determined under a variety of more catalytically relevant feedstock conditions (*i.e.* at near ambient pressures). Also determined were the cases in which elevated reaction temperature were required to allow activation of surface species.

1.2.1.1. Challenges to the analysis of nanoparticle catalysis via SFG

One significant challenge for SFG is that for nanoparticle catalysts (an important field in heterogeneous catalysis, see Section 1.5 for details) the capping agents, inherently present from the catalyst synthesis, can cause significant issues. Firstly, they are thought to block reactants adsorbing on active surface sites and, secondly, they produce interfering signals that make reaction intermediates difficult to detect.[38] One solution offered was to remove the organic capping material using UV light or solvent cleaning. For Krier *et al.* such removal of the organic capping agent, in this case of polyvinylpyrollidone for a platinum nanoparticle system (platinum/PVP nps), increased the number of active sites and allowed for detection of reaction intermediates.[38] However, Baker *et al.* suggested that the organic capping (again for a platinum/PVP np system) was dynamic and in some cases increased the catalytic activity.[39] Therefore, although removal of organic capping species might be expected to simplify or improve SFG analysis such removal is also thought to influence catalytic behaviour or reaction rates. This leads to inaccuracies in any analysis conducted in this manner.

Overall SFG provides a useful technique to learn about surface adsorbates at more catalytically relevant pressures, but is experimentally complex to carry out and is fundamentally limited by the difficulty of separating intensity changes due to geometry from those due to concentration.

1.2.2. Attenuated total reflectance infrared (ATR-IR) and diffuse reflectance infrared Fourier transform spectroscopy (DRIFTS)

ATR-IR and DRIFTS are both forms of infrared (IR) spectroscopic analysis. IR spectroscopy gives information on both the structure and environment of molecules. DRIFTS is a variation upon the traditional transmission IR spectroscopy. Use of DRIFTS for studying catalysts and absorbed molecules has increased with the widespread deployment of FTIR spectroscopy and instruments fitted with enhanced detectors. Such detectors include the mercury cadmium telluride (MCT) detector. The advantages of DRIFTS over transmission IR spectroscopy include the ease of preparation of samples, as a powder can be used without the need to compress into a disk as some catalysts cannot withstand such pressing. This is an important advantage for catalysis, as for a pressed disk it is not known if sufficient

diffusion into the pellet occurs for the catalyst to all be interacting with reactive gases during an *in situ* experiment. DRIFTS can also be used in a complementary sense, as it relies upon scattered photons, so if a species gives a poor transmission spectra due to scattering losses, its DRIFTS spectra may be better as the scattered photons carry the signal and so complementary use may be highly beneficial.[40]

ATR-IR spectroscopy is one of the most powerful, and most frequently used tools for looking at the solid/liquid and solid/liquid/gas interfaces in heterogeneous catalysis. Various advantages and disadvantages exist for this technique. The process is non-destructive and capable of giving information about chemical and geometric features at the interface. Another advantage of ATR-IR is that it can be utilised to look at kinetics of complex reactions. This takes place by quantification of product and reactant concentrations. Like Raman spectroscopy, IR spectroscopy is sensitive to molecular structure, and when correctly applied ATR can probe the interface region specifically (*i.e.* the location where heterogeneous catalysis occurs). Although it should be noted that IR and Raman spectroscopic selection rules differ. Raman spectroscopy requires a change in polarisability whereas IR spectroscopy requires a change in dipole moment. As discussed in the Chapter 2, Section 2.1.5.2, Raman spectroscopy offers advantages over IR spectroscopy in the detection of molecules which are not IR-active (*i.e*. homonuclear diatomics), as well as having the ability to tolerate water in the sample. For this reason the complementary use of IR spectroscopic techniques with Raman spectroscopy is both common and effective. The further introduction of X-ray techniques (such as Extended X-ray absorption fine structure (EXAFS) spectroscopy and X-Ray absorption near edge spectroscopy (XANES)) to Raman and IR spectroscopy can allow for probing of metal nanoparticles themselves (as well as adsorbates on their surfaces) under working conditions. The use of ATR has grown as immersion probes have become commercially available. It is anticipated that further growth might occur due to the widespread use of transmitting fibre optic materials, and as hardware and instrumentation improvements occur.[41]

1.2.3. Extended X-ray absorption fine structure (EXAFS)/X-Ray absorption near edge structure (XANES) spectroscopy

EXAFS and XANES spectroscopy are X-ray absorption techniques, and commonly achieved using synchrotron radiation.[8,42] X-ray absorption techniques are principally based upon the idea of photons being absorbed giving rise to electron-energy transitions. Such transitions differ for different elements making the technique very element specific.[8,42]

XANES spectroscopy is a tool for characterising materials, and studying adsorbates, surfaces and solids.[42] Advantages of XANES spectroscopy include specific element detection, the detection of detailed information for materials without long range order, as well as electronic information. Weckhuysen *et al.* (2004) detailed various improvements which could be made to XANES including: improvement of *in situ* cells, better quantitative analysis, and complementary use with new X-ray techniques.[42] Many publications detail use of XANES spectroscopy for *in situ* analysis of heterogeneous catalysts, and its use alongside EXAFS spectroscopy is common.[30,43–45]

EXAFS spectroscopy allows for exploration of surface catalysed processes under reaction conditions. EXAFS spectroscopy is based upon the backscattering interactions from neighbouring atoms and so it can provide information about the atoms local environment. The number, type, and distance from coordinating atoms can be distinguished.[46] The detection method used in EXAFS spectroscopy is important, as it impacts upon both the depth that can be profiled and the ability to record measurements *in situ*. If the X-ray absorption is quantified using auger electrons and secondary scattering electrons, then total electron yield (TEY) can be used. When surfaces are probed using the TEY mode, the region studied is reduced to a few nanometres. This allows for relatively good surface sensitivities, which is an important factor in the analysis of heterogeneous catalysts. To demonstrate how these techniques are used *in situ* in detail, the complementary use of EXAFS and XANES spectroscopies, for the study of heterogeneous catalysis, is described as an example within the case study below.

Case study

Hard X-rays are often used to elucidate elemental structure. Material structure-function relationships are the determination of structure at the same time as properties that influence its function or activity. One such example is that a catalyst's structure might be studied as a function of its performance *e.g.* activity or selectivity. Understanding such material structure property relationships is very important in catalysis, as a catalysts performance may be directly related to its atomic structure. Reaction conditions may cause structure variations, understanding this allows for systematic variation and possible enhancement of the catalytic properties. X-ray spectroscopic data can therefore be used as part of the deduction of material structure-function relationships. In catalysis amorphous and crystalline high surface area materials often exist beside each other. XANES and EXAFS spectroscopies can be used to determine the materials structure, as the catalysts performance is measured, allowing structure and materials properties to be determined

simultaneously.[47–50] For this reason many groups have made *in situ* cells for conducting both EXAFS and XANES spectroscopies, and several considerations have been determined important in cell design. Such considerations include flow dynamics, energy range and signal-to-noise. The work of Hanneman *et al*. demonstrated a cell design that could be used across wide temperature ranges (from 123 to 973 K) and record both fluorescence and transmission signals.[51] A detailed description of the cell can be found within the publication, however, in general the cell was capable of operating on-line both in the gas- and liquid-phase. X-ray absorption spectroscopy (XAS), EXAFS and XANES spectroscopies, and in addition XRD were used to analyse the catalyst within the cell. Mass spectrometry or IR spectroscopy was used to analyse the effluent stream in the gas or liquid phase respectively. The catalyst studied could be powder or a self-supporting wafer.

The cell was tested for a series of studies with the aim of elucidating structural information about working catalysts. Three studies were chosen, each chosen as they allowed data to be recorded at three differing beamlines. This was a function of the differing edge energies of the elements for the EXAFS measurements of the three examples. This allowed for a thorough evaluation of the cells capabilities and limitations across a variety of conditions.

Firstly, flame spray pyrolysis monometallic and bimetallic catalysts, containing 0.1% platinum or gold with 0.1% of either palladium, rhodium or ruthenium were investigated in the cell with *in situ* XANES, during heating from 123 K under 5% hydrogen/helium. This enabled the temperature at which the metals reduced and the extent to which alloying occurred to be identified,[51] and compared with other literature examples.[52–54] This was supported by fitting of the Fourier transformed (FT) fluorescence EXAFS spectra.

Secondly NO_x storage and reactivation was tested for a platinum/barium/cerium dioxide catalyst. Oxidised metal and products of thermal decomposition were detected suggesting a reduced capacity for NO_x storage.[55] Catalyst reactivation, monitored by XRD, confirmed the conversion of barium to barium nitrate. The use of XAS fluorescence indicated the expected change in oxidation state had taken place for the platinum during NO_x storage and reactivation.

The final example explored was that of gold/copper oxide catalysts for liquid phase alcohol oxidation. Activity structure relationships were explored using XAS and IR spectroscopy with reduction of the initially oxidised gold to the metallic state taking place on exposure to the reaction mixture. A slight increase in activation was seen and attributed to acetophenone formation as characterised by IR spectroscopy.

Overall the cell performed well for low metal concentrations during both static and dynamic gas conditions. The performance was maintained for a range of temperatures, covering most temperatures required for spectroscopic analysis in catalysis. The cell could find application for a wide range of elements, and worked for different gas phase and liquid reactions. Overall this paper illustrated the suitability of EXAFS and XANES for *in situ* analysis of heterogeneous catalysts. This further exemplified the potential advantages of these techniques. It is our intention that such techniques would be used in a complementary sense with TIR Raman spectroscopy.

1.2.4. Near ambient pressure X-ray photoelectron spectroscopy (NAP-XPS)

XPS uses the photoelectron effect to produce emission spectra. These spectra correspond to the electronic energy level to vacuum level transitions in the molecule. High pressure XPS, also known as near ambient pressure XPS (NAP-XPS), has become achievable due to advances in vacuum and analyser techniques and design, with synchrotrons providing high flux X-ray photon sources. This was a major advantage as it has allowed pressures near to those at which many catalytic reactions take place to be reached. This technique allows for the study of surface chemistry and elemental composition. There has been particular success at examining systems where there have been several options for the active state of the catalyst.[8] An example of the use of NAP-XPS for the understanding of heterogeneous catalysis under more realistic conditions is given in the case study below.

Case study

Real catalysts often consist of small particles, which expose different atomic terminations. A real catalyst surface may, therefore, have a high concentration of step edges, kink sites, and vacancies. Such features are often considered catalytically active.[1,56] Correspondingly, a good model catalyst should be able to reproduce such features. Stepped single crystal surfaces have well defined surface structures and can be prepared, for example, with a vicinal surface. In such cases two high index surface functional groups are bonded to two adjacent atoms giving a high concentration of such sites. Stepped single crystals are, therefore, often used as models for such catalyst behaviour. Another related question is the effect of adsorbates on the surface structure, as has been observed under UHV conditions.[57–59] However, as mentioned previously in this report, UHV conditions do not always reproduce results obtained under actual operating conditions. It is of importance to examine the structural and chemical changes that take place under realistic operating conditions. Tao *et al*. used NAP-XPS in conjunction with scanning tunnelling microscopy (STM) to examine a single crystal

stepped platinum surface under high (not UHV) pressures (0.1 Torr of carbon monoxide).[60] An absorbing gas of carbon monoxide was chosen due to its widespread use in industrial catalysis and processes such as carbon monoxide oxidation in automobile catalytic converters. NAP-XPS and STM allowed for the determination of oxidation state, chemical nature of adsorbates, and atomic structure for the catalyst surface, under more realistic operating conditions. The use of STM imaging allowed changes in the surface structure to be monitored at similar gas pressures. This provided a method for following changes, such as the terrace width and step height variations, as the carbon monoxide pressure was varied. Complementary to this, NAP-XPS was taken under various pressures, and the varying intensity attributed to the changing concentrations of surface platinum atom sites on the cluster edge. This technique also allowed for examination of the coverage of carbon monoxide as the gas pressure was varied. This gave a method for attributing the changes in the carbon monoxide concentration to the structural variations seen by STM. This led to the conclusion that as carbon monoxide absorbs, at low pressures, subsequent restructuring of the surface steps occurs. This had been observed previously by Pearl *et al*. and was attributed to changes in the energetics of the electrons as well as the elastic interactions between steps on the surface.[61] Further to the ability to reproduce results at low pressure, at high pressures, Tao *et al*. reported the reversible formation of triangular nanoclusters – platinum atoms that have been pulled out of the surface into small clusters.[60] It was postulated that the high carbon monoxide concentration, as determined by NAP-XPS, led to strong repulsions between the carbon monoxide molecules. The formation of the nanoclusters was driven by this repulsion, as it allowed the carbon monoxide to sit on low coordinate edge atoms. In these positions the carbon monoxide molecules tilted away from the other adsorbed molecules reducing the repulsion they experienced. This led to the formation of the observed triangular nanoclusters.

Density functional theory (DFT) was used to determine if the energetics of the system supported the experimental data. The most favourable structures at various pressures were calculated. The calculations agreed that at high pressures a triangular nanocluster would represent the lowest energy structure. The adsorbed carbon monoxide would then fan out on the edges of this nanocluster, to reduce repulsion between the adjacent carbon monoxide molecules. This led to the decreased energy of this structure. The low coordination platinum site and high carbon monoxide coverage, suggested by DFT, were consistent with the experimental results.

Overall the complementary use of NAP-XPS and STM allowed for determination of the large scale restructuring of the surface, which was seen for large coverages of adsorbates. The example illustrates the ability of, and the important results determined from, systems which take into account the stepped nature of the catalyst as well as allowing operation under realistic operating conditions. NAP-XPS is therefore an important tool in furthering understanding of the behaviour of real heterogeneous catalysts. It is the intention in this project that such techniques could be used in conjunction with TIR Raman spectroscopy.

1.2.5. Summary of the use of *in situ* techniques for studying heterogeneous catalysis

A variety of techniques for the *in situ* study of heterogeneous catalysts have been surveyed. The advantages and scope for complementary use with TIR Raman have been highlighted. The limitations of these techniques has also been discussed, such as the difficulties of SFG in providing quantitative information when other factors such as adsorption geometry change simultaneously. This sets the scene for understanding the place Raman spectroscopy (and in particular TIR Raman) sits within the current range of *in situ* techniques available. This will be discussed in more detail within the two sections which follow.

1.3. Raman Spectroscopy with *in situ* heterogeneous catalysis

1.3.1. Why use Raman spectroscopy?

Raman spectroscopy is a technique that allows probing of all phases including mixtures and can in principle be employed over wide temperature and pressure ranges (-273 to >1000 °C, and 10^{-7} to > 10^{6} Pa). The spectra obtained can provide molecular level information.[62] The suitability of Raman to the field is partly due to its ability to complement other surface sensitive techniques (Table 1.1). Techniques such as SFG, and ATR-IR are often combined with Raman and TIR Raman spectroscopy in a complementary fashion.[63] It can also be noted that Raman spectroscopy has certain advantages over techniques such as UV spectroscopy and electron energy loss spectroscopy (EELS). For example although EELS can provide detailed molecular structure information, similar to Raman spectroscopy, it can only be operated under UHV conditions. This does not allow for bridging of the pressure gap. Equally, for UV spectroscopy the chemical sensitivity is low, particularly if a mixture exists, although the use of elevated pressures is relatively straightforward.

Raman spectroscopy does, however, have some limitations. Firstly, the sensitivity of Raman spectroscopy is generally low, particularly if the loading of the catalyst active material is low (which is often unavoidable). To overcome this intense laser beams are used to improve the number of Raman scattered photons. However, the laser light used for excitation can cause

damage to the sample, such damage is irreversible and will prevent spectra from being taken in that region of the sample. It may also produce misleading results. Finally, fluorescence from the sample, substrate or contaminants in the sample being probed can weaken or obscure Raman bands.[64,65]

Table 1.1. Table to show comparison between capabilities of a range of techniques, for which Raman and TIR Raman spectroscopies can be used in a complementary sense with, or can provide an advantageous alternative. Surface sensitivity values for TIR Raman and ATR-IR spectroscopies were calculated from for the air silica interface at 73°. For the value for TIR Raman spectroscopy, calculations were made for a laser wavelengths of 660 nm. For ATR-IR spectroscopy a wavelength of 4000 nm (or 2500 cm^{-1}).

	SFG	TIR Raman	Bulk Raman	ATR-IR	SERS	UV	EELS
Surface sensitivity:	Intrinsically.	Fair, better than ATR-IR (function of λ) – probing depth 54 nm.	Moderate depending upon the lens.	Reasonable, probing depth 652 nm.	Large enhancements when on or near surface.	No.	Yes ≈ 0.1 µm.[66]
Quantification:	No.	Good.	Good.	Good.	Good.	If absorbs in UV can calculate concentration.[67]	With suitable spectrometer.[66]
Geometric effects:	Very sensitive (if known quantity).	Poor.	Poor.	Difficult.	Possible?	No.	Yes.
Focus on small/controllable areas for kinetics:	Good.	Good.	No.	Not good (IRE elements typically large).	-	No.	Yes.
Materials transparent to incoming and outgoing signal:	Typically IR/vis needed.	Near excitation; fluorescence a problem, usually visible.	Near excitation; fluorescence a problem, usually visible.	IR near signal of interest.	Visible, limited to suitable SERS substrates.	UV.	Vacuum.

1.3.2. Literature use of Raman spectroscopy to study heterogeneous catalysts *in situ*

This section aims to detail some of the work of others using different types of Raman spectroscopy (not including TIR Raman spectroscopy) for *in situ* studies of heterogeneous catalysts. No previous publications exist for the use of TIR Raman spectroscopy for *in situ* heterogeneous catalysis. One common use of Raman spectroscopy has been to study the surface of metal oxide heterogeneous catalysts such as zeolites, layered hydroxides, and supported metal oxides.[62] It is worth noting that compared to nanoparticles these samples generally exhibit higher thermal stability and so illumination with intense laser beams is less likely to result in laser induced damage. The examples given in the section below focus on the study of such metal oxide catalysts. These examples are not exhaustive, and do not necessarily represent contributions in order of importance to the field (as this is somewhat debatable), but are intended to give a flavour of the types of experiment that have been used in this area.

1.3.2.1. Operando Raman spectroscopy

Operando and *in situ* techniques share similarities, and although the differences between the techniques are not consistently described in the literature a general distinction can be made between the two. For example the use of *operando* Raman spectroscopy is often considered as the:

"simultaneous *in situ* Raman spectroscopic observation of the catalyst and online reaction product analysis (*e.g*. mass spectrometry, IR spectroscopy, Gas Chromatography (GC) *etc*.)."[62]

The subject was first discussed extensively in 2002,[68] but has since been the subject of many more publications, that have demonstrated the ability for Raman to be used in a variety of areas.[69,70] *Operando* Raman spectroscopy has been used to elucidate the presence of surface species and intermediates, and has led to improved catalyst design.[71,72] This was achieved by spectroscopic investigation of the catalysts' active sites. The most common use of this technique is in methanol oxidation, where various different catalysts have been studied. Two such examples using molybdenum-based catalysts are reported by Brandhorst *et al*. and Guerrero-Perez *et al*..[73,74] Brandhorst *et al*. used Raman-IR spectroscopy with online GC to study a supported catalyst (MoO_3/Al_2O_3).[73] Surface intermediates were detected by IR spectroscopy, and the surface molybdenum hydroxide species by Raman spectroscopy. The

appearance and disappearance of these species was then correlated with the conversion of methanol to formaldehyde, methyl formate, and diethyl ether determined by GC. Guerrero-Perez *et al*. studied a tungsten-molybdenum catalyst during oxidative dehydrogenation of propane to propylene with the intention of improving propylene selectivity.[74] The phases that gave the best product yield were identified. From this the selectivity was enhanced giving targeted and improved catalyst design.

1.3.2.2. Quantitative Raman spectroscopy

Raman spectroscopy can, in some configurations, be used quantitatively.[75–77] Raman scattering cross sections result in the number of Raman photons observed being linear with concentration, the exception being when absorption occurs such that either the excitation photon flux is not uniform through the sample, or the scattered photons do not have an equal chance of being emitted from different depths within the sample. In such cases consideration must be given to what fraction of the sample is actually being probed.

1.4. TIR Raman, and its applicability to *in situ* studies of heterogeneous catalysis

TIR Raman spectroscopy is a variant of Raman spectroscopy for which an evanescent electric field acts as the excitation source.[78] TIR Raman spectroscopy offers a range of potential advantages over standard Raman spectroscopy, which reduce or avoid some limitations of the bulk technique.[79] The likelihood of laser induced sample damage is reduced in TIR Raman spectroscopy. This is due to the nature of the technique as the laser is reflected and not absorbed, within the sample bulk, and so excessive heating is much more limited (Section 2.1.5). Another potential advantage is that the size of the sample spot, provided by the laser, can be increased without having to change the sampling depth. This can result in a smaller compromise in sample power for a given sampling depth, as the likelihood of laser induced damage is reduced. Accordingly higher laser powers can be used, and an improved signal to noise ratio is acquired.[80] The IR spectroscopic probing depth in ATR-IR spectroscopy is significantly larger than that in Raman spectroscopy (Table 1.1). A discussion of the calculation of probing distances can be found in the Appendix. A shorter probing distance relates to a higher surface sensitivity, than the bulk or gas reagent sensitivity, as surface species alone are likely to be probed. Better surface sensitivity is, therefore, seen for Raman rather than IR spectroscopy. There are, however, disadvantages of Raman that apply equally to TIR Raman spectroscopy. The main disadvantage seen is fluorescence. Fluorescence still occurs in TIR Raman spectroscopy and is detrimental just as it is in bulk Raman spectroscopy. Measures can be taken to reduce the effect, such as careful selection of the substrate or the excitation wavelength.[78] It is also possible to time gate out Raman spectroscopy, a fast effect

which takes advantage of fluorescence being a slower effect.[81,82] However, time gating has not been done for TIR Raman spectroscopy as it is both expensive and technically ambitious. Sensitivity is also still an issue in TIR Raman spectroscopy. However, the restriction of the evanescent wave to the area of interest can contribute to improved surface selectivity.

Although TIR Raman spectroscopy holds potential advantages its use is less common than its IR counterpart ATR-IR spectroscopy which also uses an evanescent wave. This can in part be attributed to the widespread use of surface enhanced Raman scattering (SERS) spectroscopy a surface sensitive technique which allows for enhanced sensitivity in Raman spectroscopy due to specific attributes of the material's surface and molecules present at the surface.[83] However, SERS spectroscopy cannot be used in all cases, and restrictions are placed upon the substrates and materials that can be studied. Examples of such restrictions include: that the substrate must support a surface plasmon resonance, the species to be analysed must sit within a few nanometres of that support, and for transition metal species it is desirable to look at metals (such as copper or gold) that can support plasmons in the visible range and are resistant to corrosion.[84] Quantification in SERS spectroscopy is also heavily reliant upon the substrate and so can be inherently unreliable, especially for *in situ* work where the SERS substrate, and consequently the enhancement factor, can change on exposure to different reaction conditions. For TIR Raman spectroscopy such restrictions do not apply and the only substrate restrictions are that it should not fluoresce and should be transparent around the wavelength of the excitation and Raman scattered light.[78] If fully exploited TIR Raman spectroscopy could be used in cases which are not suited to SERS.[78]

1.5. Nanoparticles as a model catalysts

Developing a suitable model catalyst was of importance in interrogating catalyst properties. The complexity of an industrial catalyst, can make interpretation of spectroscopic data and correlation with kinetics difficult due to the range of particle sizes, shapes, and additives which may be present. The differences in actual catalyst behaviour due to differences in the materials properties used is known as the materials gap. The materials gap is related to both structural and compositional differences between a real industrial catalyst and a well-defined model catalyst.[16] One implication of the materials gap is that traditional kinetic studies vary significantly depending upon catalyst preparation, hence generalisation is not possible. A model catalyst can allow for the spectroscopy and kinetics to be measured on a well-defined system, allowing results to be better understood and expanded upon (and possibly in turn allowing meaningful studies of the practical catalyst to be performed).[8]

Nanoparticles offer advantages over traditional catalysts, as they allow accurate control over properties such as size and shape.[85–89] This can result in monodisperse rather than polydisperse nanoparticle systems.[90] Such control is important as surface structure is known to have significant impact upon catalytic rates and activities.[33,91–94] Much work has been conducted, looking at colloidal systems as model catalysts.[95–97] The area is claimed by some as the forefront of creating controlled property catalysts.

In order to generate nanoparticles for use as model catalysts, it is instructive to briefly review the factors that control their synthesis. For colloidal synthesis this can generally be split into nucleation and growth processes. The following sections highlight how careful control of factors that affect these phenomena enable the controlled synthesis of particles with desirable properties. These properties include size control (monodispersity) or composition control.

1.5.1. Methods of synthesising nanoparticles

1.5.1.1. Top-up and bottom-down synthesis

Various methods for nanoparticle synthesis exist. Broadly the topic can be divided into bottom-up and top-down approaches. Bottom-up approaches take smaller building blocks such as atoms or molecular components and combine them. Typically this takes place in the liquid or gaseous phase, to form nanoparticles.[98,99] If such processes proceed in the solution phase they generally include dissolution and precipitation stages. Liquid phase examples include co-precipitation by metal reduction. In such processes stabilising agents are used to prevent rapid agglomeration. In the case of bottom up approaches these stabilising agents can deliver control either by charging (electrostatic repulsion) or steric effects. In the latter case capping agents are used. Top-down approaches involve the breaking down of larger particles, and most examples found in the literature are physical processes such as milling.[100] The work of Xia and Wang illustrates methods to prepare nanoparticles in both a bottom-up and top down manner.[101] The bottom-up approach utilised thermal decomposition of bismuth acetate in solution with polyvinylpyrrolidone capping agent. The top down approach, in contrast, added a bismuth powder to a hot solvent. This resulted in melting of the powder to give large droplets. Stirring and emulsifying then broke the large droplets down to smaller more monodisperse nanoparticles. This approach is represented schematically in Figure 1.3. Bottom-up approaches are generally considered as more promising due to the inherently higher levels of control over nanoparticle formation. This leads to greater control of the properties of particles produced.

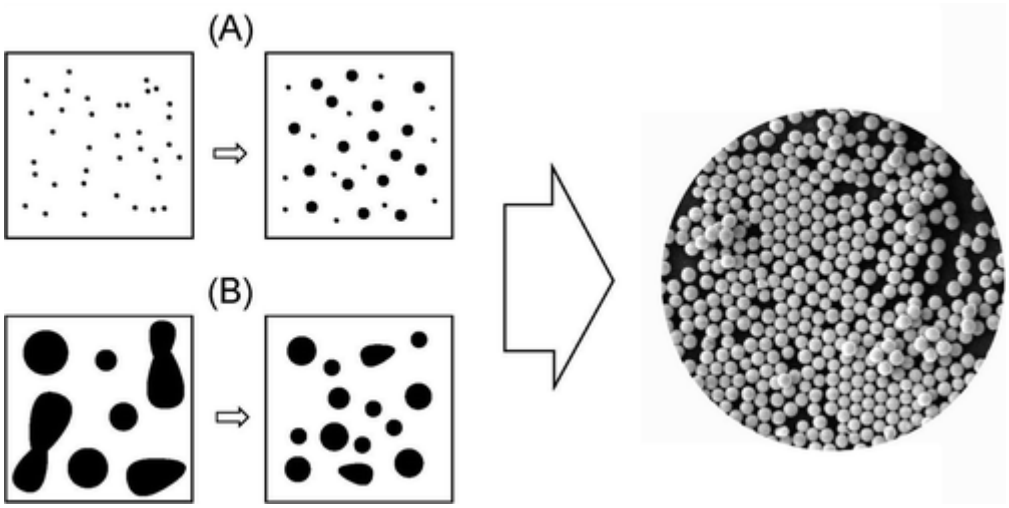

Figure 1.3. Schematic of chemical A) top-down and B) bottom-up synthetic routes to nanoparticles. Reprinted with permission from Wang, Y. & Xia, Y. Bottom-Up and Top-Down Approaches to the Synthesis of Monodispersed Spherical Colloids of Low Melting-Point Metals. Nano Lett. 4, 2047–2050 (2004). Copyright 2004 American Chemical Society.

1.5.1.2. Metal salt reduction

A widely used bottom up approach to nanoparticle synthesis is metal salt reduction.[102–106] A generic scheme for the process is given in Figure 1.4. A metal salt, comprised of a non-zero valent metal atom, was reduced to the metal oxidation state. Various methods of reduction can be utilised, one example being the use of strong reducing agents which are thought to aid quick or burst type nucleation. Thermal assisted reductions,[107–111] a variant of metal reductions, typically use a refluxing solution of a high boiling point solvent. A coordinating reducing capping agent, or additional reducing agent species, brings about the metal reduction. Once the metal is reduced, the nucleation and growth processes can take place resulting in the formation of a nanoparticle. Further aggregation to the bulk metal thermodynamic product is prevented by the use of a capping agent.

$$nM^{x+} + nx(e^-) + \text{capping agent} \longrightarrow nM(\text{capping agent})$$

Figure 1.4. A generic scheme for metal salt reduction for the creation of nanoparticles.

1.5.1.3. Capping agents

The primary role of a capping agent is to prevent aggregation. They provide stabilisation of the metal nanoparticle, as shown in Figure 1.5. Capping agents can be classified as either steric or charge stabilising (it is quite common for capping agents to display a mixture of the two).[112–114] With moieties such as bulky organics (*e.g*. oleylamine or dodecanethiol) providing

steric stabilisation and charge stabilisation being provided by the presence of strongly electron donating or withdrawing groups (*e.g.* cetrimonium bromide). One common example is polyvinylpyrrolidone which is one of the most commonly used homopolymers to stabilise nanoparticles. Part of its success is likely to stem from its ability to satisfy both steric and ligand requirements. Polyvinylpyrrolidone is sterically bulky with an M_w of several 1000 a.m.u. (*e.g.* 55,000 a.m.u. was used in the present work), but also contains pyrrolidone nitrogen groups that can bind to the metal.[56] Many other alternative polymers and biopolymers have also been used, such as polyvinyl acetate,[115] cellulose,[116,117] polysaccharide,[118,119] and poly acids.[120,121] Organic capping agents are not limited to conventional polymers; a number of other molecules such as dendrimers,[94,122] ligands,[123,124] micelles,[125,126] and surfactants can also be used.[127,128] A variety of commonly used capping agents are given in Figure 1.6.

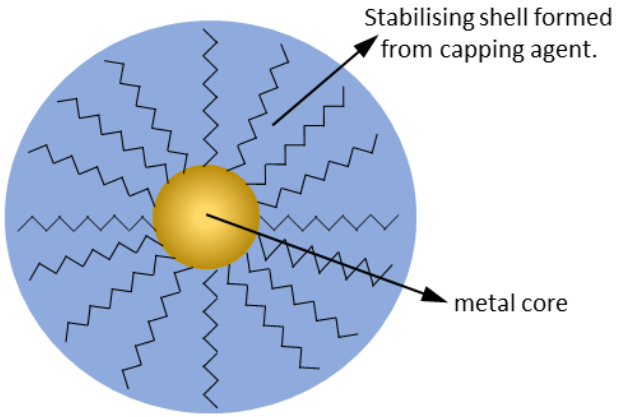

Figure 1.5. Schematic representation of the stabilisation (steric or electrostatic) provided to metal nanoparticles by a capping agent.

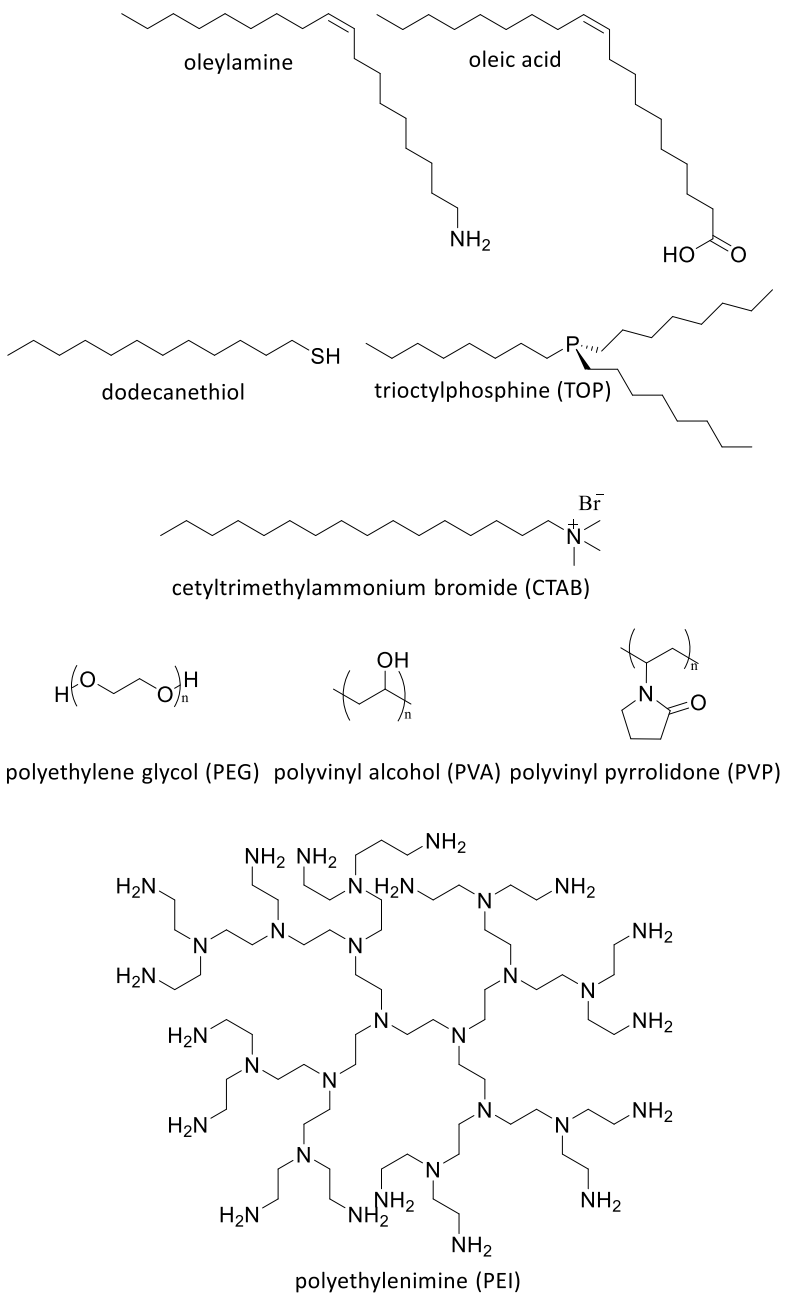

Figure 1.6. Examples of structures of capping agents commonly used in nanoparticle synthesis, including long chain hydrocarbons, surfactants, polymers, and dendrimer capping agents.

1.5.1.3.1. Capping agents and catalysis

A key question when employing nanoparticles as catalysts or catalyst models, is whether organic capping agents affect the catalytic reaction taking place at the metal surface. Until recently the viewpoint has been that the organic capping agent blocks some surface metal sites. This reduces the metal surface area available, which in turn reduces the efficiency of the catalyst.[129] For this reason (and because of possible interference with the spectroscopic techniques used to probe catalytic species, such as SFG – see Section 1.2.1) many groups aimed to remove the organic capping agent before using the nanoparticles as catalysts.[115,130] However, the possible promoting effects of capping agents for nanocatalysts has also been noted in a number of cases.[131–135] In 2012 the work of Baker *et al*. suggested that in fact the organic capping agents (in this case polyvinylpyrrolidone and oleic acid) could, in some circumstances, act to increase the activity of the catalyst.[136] They concluded that the organic capping agents were dynamic species that did not prevent catalysis. Further work by other groups also provided indications of such dynamic behaviour. One example is the work of Roy and Bhattacharya in 2013,[137] in which the authors used polyvinyl alcohol as a capping agent for platinum nanoparticles with differing particle sizes and capping agent concentrations. They found that when the capping agent concentration was increased a decrease in the particle size was seen, with an increase in the particle diameter giving an increase in the catalytic activity for the alkaline oxidation of methanol. This was the opposite of the usual trend observed. Conversely, when the capping agent concentration was not changed a decrease in catalytic activity was seen. This was seen for an increased particle diameter due to lower surface area. This may in turn correspond with Baker's notion of a dynamic capping agent, which changes the properties of the catalyst, rather than simply acting as a spectator.

It is clear further work is needed to understand better the role of the organic capping agent in nanoparticle catalysis, but they provide an effect route to access an important class of model catalyst materials. Capped nanoparticles will be utilised throughout this work.

1.5.2. Nanoparticle growth and nucleation

Nucleation is the first stage in nanoparticle formation from a previously homogeneous system. In general we know that precipitation can occur if a factor that changes the solubility of a species is varied. Examples of such variables include concentration or temperature. It is this process that governs the nucleation of the precursor species during the synthesis of metal nanoparticles. This formation of small crystallites of the precursor (or reduced metal) is the process of nucleation. This is followed by crystallite growth. This process is summarised below in Figure 1.7.

Inducing nucleation does not, however, guarantee nanoparticles will form or will be monodisperse. One important parameter is the relative rate of the nucleation and growth stages. Fast or burst type nucleation,[138,139] as the name suggests gives rapid access to many nucleation sites, before significant growth can occur. After the nucleation burst the conditions change so that no further nucleation occurs, but only particle growth. If growth then occurs at the same rate from particles nucleated at the same time, for example by the mechanism discussed below, then the formation of uniformly sized particles can take place. This is known as the La Mer mechanism.[138] The creation of monodisperse particles from a slower nucleation stage, leading to simultaneous nucleation and particle growth, can be more difficult. This is due to new small nuclei which may still be being formed, after some have grown to an appreciable size. An energetic basis for an understanding nucleation can be gained from classical nucleation theory.[140]

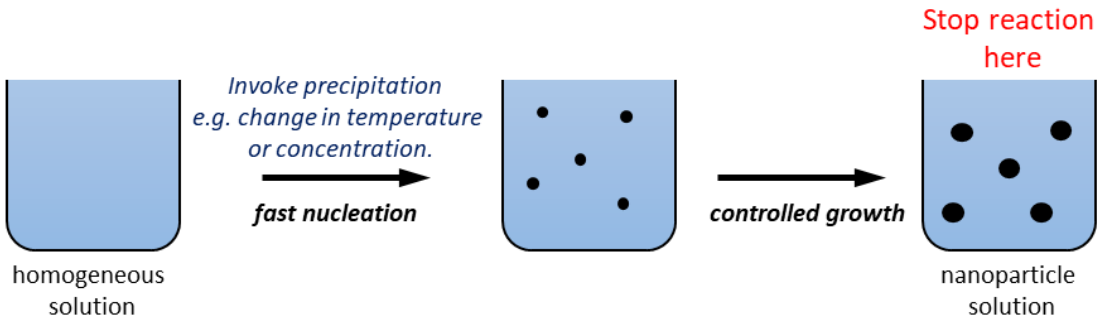

Figure 1.7. Simple schematic of nucleation and growth process from a homogeneous reagent solution.

1.5.2.1. Classical nucleation theory

Classical nucleation theory predicts that the total free energy cost ΔG_{tot} of forming a nucleus for a spherical crystal, with radius r can be modelled by Equation 1.1.[141]

$$\Delta G_{tot} = \Delta G_v + \Delta G_s = \frac{4\pi r^3 \rho \Delta\mu}{3} + 4\pi r^2 \gamma \qquad \textit{Equation 1.1}$$

Where ΔG_V is the bulk volume contribution, ΔG_s is the surface free energy contribution, γ is the interfacial free energy, ρ is the density of the bulk liquid, and $\Delta\mu$ is the difference in chemical potential between the bulk solid and bulk liquid.

It can be seen that the bulk volume term in Equation 1.1 scales as r^3, whereas the surface term scales as a function of r^2. This is shown graphically in Figure 1.8. The bulk term is always negative and therefore energetically favourable. This is due to the strong metal-metal bonds which exist in the bulk cluster. The interfacial free energy is always positive and therefore not favourable. As given in Equation 1.1, the total free energy is a sum of these energetic

two contributions. This means that for particles of sufficiently small radius the interfacial free energy will dominate, and the total free energy will be positive. In practice in the case of nanoparticles, capping agents are often present, which may reduce significantly the surface free energy term. This may perturb this simple picture by stabilising the interface between small particles and the liquid phase, but this is not currently well understood.

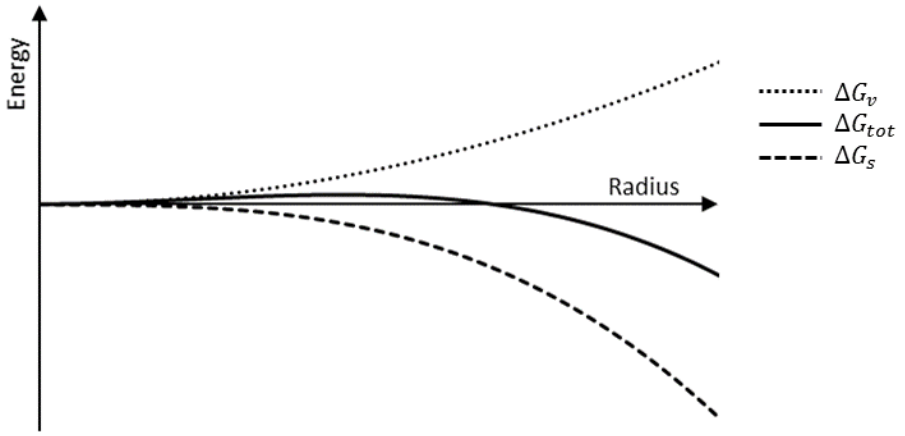

Figure 1.8. Graphical representation of volume and surface contributions to total free energy as a function of particle radius.

1.5.2.2. Classification of growth mechanisms

Nucleated particles will grow in the reaction medium. Such growth is complex, and can be controlled by factors such as reaction or diffusion limitation or binding to templating agents. The growth that occurs first is due to the existing nuclei which act as growth sites for remaining metal in solution. Ripening can then occur *via* the following mechanisms: Ostwald ripening and digestive ripening.

1.5.2.3. Ostwald ripening

The early work of Wilhelm Ostwald, focused upon the nucleation of crystals in droplets. This gave rise to the observation that less stable polymorphs will nucleate first, and will later convert to the more stable polymorph.[142] More importantly for this work, Ostwald's observations of saturated solutions also led to the conclusion that such solutions, once left to equilibrate, invariably contained significantly more large particles than small. It was also noted that enhanced solubility resulted from the grinding of particles, which produced increased surface area and therefore higher surface free energy.[143,144] The combination of these principle ideas led to the conclusion that in a closed system small crystals will dissolve and large particles will continue to grow. This growth occurs using the material resulting from the preferential dissolution of the smaller particles.

1.5.2.4. Digestive ripening

Digestive ripening achieves the reverse of Ostwald ripening, or at least the control of particle size by gradual reduction in the particle dispersity towards a thermodynamically favoured size for the system of particle plus stabilising agent. In the case of nanoparticles this is often achieved by the refluxing of a nanoparticle solution in the presence of excess surface active capping agent. This is often known as a Digestive Ripening Agent (DRA). Use of a DRA leads to of the favouring of a particular particle size at which the surface-capping agent interactions are strongly stabilising. Digestive ripening then occurs through the break-up of large particles, and the increase in size of small particles, until a more monodisperse size distribution is achieved.[145,146] The breaking of larger more thermodynamically stable particles may seem counterintuitive. However, in the presence of a DRA the strong metal to ligand (capping agent) bonds on the particle surface lead to the enhanced thermodynamic stability of smaller particles. This is due to optimisation of the balance of the surface area (for metal-capping agent binding) and the metal-metal bulk bonding contributions. Defects present within larger particles are known to induce stresses capable of causing bond rupture. Given the thermodynamic drive in the presence of a DRA to smaller particles, such defects could have an impact upon the kinetics and rate of small particle formation.[145]

Growth mechanisms for digestive ripening originated from studies of gold metal clusters, and alkane thiol DRA groups.[146] The method has subsequently been expanded for a range of metals (including copper),[148] and ligands such as amines,[149–152] and phosphines have proved effective.[153] Originally, digestive ripening was seen to take place *via* a three stage process known as solvated metal atom dispersion (SMAD). Firstly, the as formed colloidal particles were added to the DRA. Secondly the capped nanoparticles were separated from the other reagents and the products by precipitation. Finally the capped nanoparticles were refluxed in the DRA.[145] However, it was seen that the same process may lead to particle control, in systems where the separation of these steps is less well-defined. Kim *et al*. described an alternative system in which digestive ripening was seen, where no additional precipitation stage was required.[124] The synthesis gave small (3.5 nm) monodisperse palladium nanoparticles, *via* the thermal decomposition of a metal precursor, which was aged at 300 °C in the presence of trioctylphosphine. A digestive ripening type mechanism was proposed, based upon the TEM images recorded for variation of the ripening time. Ripening time is the term given to the period in which the reduced metal is held at a fixed high temperature. This allows for particles to grow or ripening to occur. In their work, particle size distributions shortly after the initial metal reduction (nucleation) were polydisperse with small irregular

shaped nanoparticles, while longer ripening times gave rise to smaller particles, with regular spherical shape and improved monodispersity. Zhang *et al*. summarised this effect,[154] and described digestive ripening as nanoparticles:

"Prepared by a SMAD (solvated metal atom dispersion) method or the chemical reduction of metal ions. The size distribution of these nanoparticles is then narrowed by refluxing the nanoparticles with a large excess of digestive agents in an argon-blanketed solvent for an extended period of time."

1.5.3. Introduction to the synthesis of small, stable, and size controlled copper nanoparticles

As described in Chapter 4 the use of copper nanoparticles as a model catalyst is one major focus of this thesis. Over the years there has been a drive for the synthesis of small, high surface area, nanoparticles with a high degree of size uniformity or monodispersity. This has been achieved for a number of different metals, such as silver, gold and platinum.[155–157] Copper is a metal of interest due to its low cost and high catalytic activity.[158–161] The synthesis of metallic copper nanoparticles has been less commonly carried out, due to the ease of oxidation of copper, into the copper(I) or copper(II) oxidation states. The formation of copper oxide nanoparticles is more common, but these are difficult to reduce to the metallic oxidation state without sintering and agglomeration (in part due to a large volume change).[162–164] Instead, the focus of this work is to produce metallic copper nanoparticles. A surface layer of oxide may be present in such systems, usually as a result of post synthesis handling, but is more easily reduced than a nanoparticle where all the material is copper oxide and a large structural or volume change is required. A schematic depicting the size dependency of copper nanoparticles upon oxidation state is given in Figure 1.9.

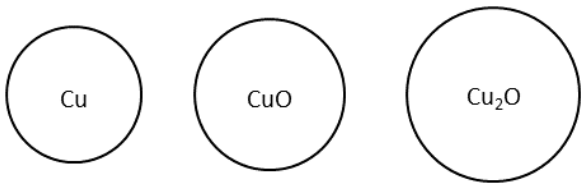

Figure 1.9. 2D representation showing the change in diameter of spherical copper particles as a result of volume change on oxidation – the same quantity of copper being present in each case. Literature densities of 8.51 g cm^{-3}, 6.31 g cm^{-3}, and 6.00 g cm^{-3} (values from CRC Handbook of Chemistry and Physics) for copper (Cu), copper(I)oxide (Cu_2O), and copper(II)oxide (CuO) along with their M_w values imply a volume ratio of 1 : 1.19 : 1.21.[165]

Metallic nanoparticle synthesis by metal salt reduction, as described in the Chapter 2, goes *via* the reduction of the metal to the zero valent oxidation state.[104,105] Unlike many nanoparticle systems in which the metal is not so readily oxidised, copper undergoes

oxidation very readily. In some cases this oxidation can create a problem by occurring after reduction of the metal salt but before the formation of nanoparticles as shown in Figure 1.10. This prevents nanoparticle formation because the oxidised species produced are generally stable in molecular form. This is highly detrimental to the formation of nanoparticles in considerable yields.

Conversely a similar process that might occur, but does not affect nanoparticle yield, is the oxidation of as-formed nanoparticles to give a copper oxide shell. Since this happens on the surface of the formed nanoparticles after their synthesis, it does not prevent their formation and if the solid copper oxide is stable to dissolution will not lead to decomposition. Stable copper nanoparticles with a visible oxide shell are reported in a number of literature examples.[166–168] Although few examples of copper nanoparticles with very small or very well controlled particle size have been seen. These processes are summarised in Figure 1.10.

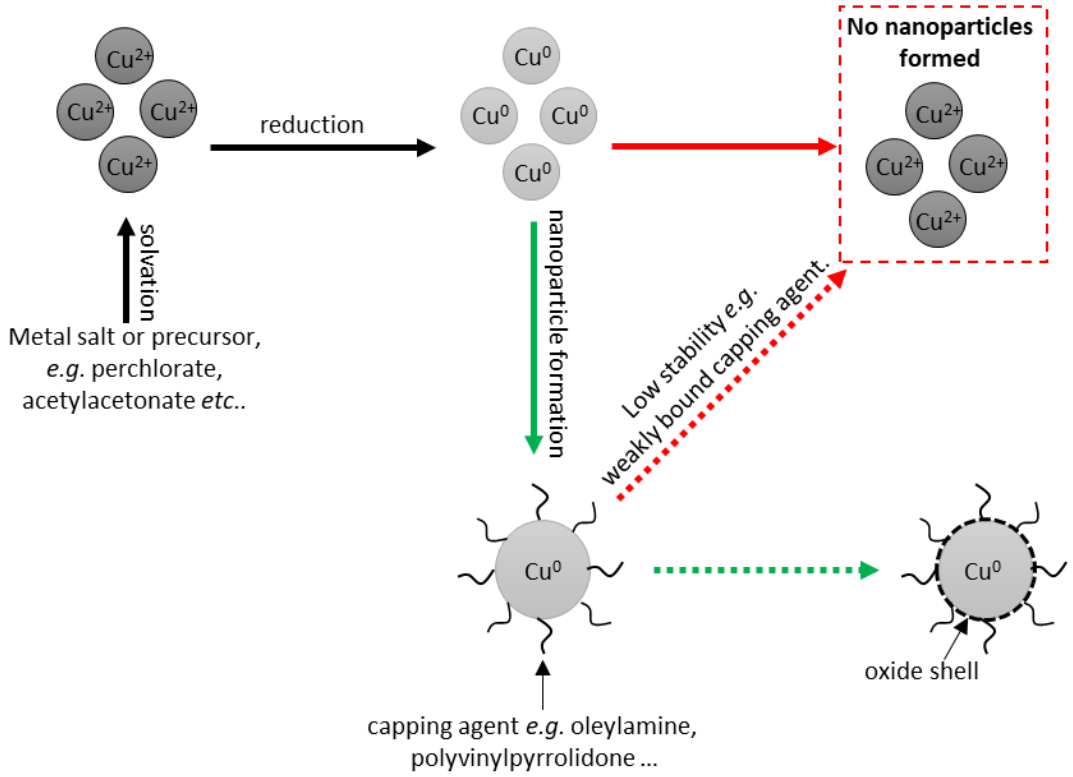

Figure 1.10. Diagram to show how ease of oxidation of copper metal can lead to either metal re-oxidation, metal nanoparticle decomposition, where no stable particles are formed, or to the formation of stable oxidised nanoparticles.

1.5.3.1. Methods for the creation of small, stable, and size controlled copper nanoparticles

Methods from the current literature for synthesis of small (sub 10 nm) as well as monodisperse copper nanoparticles will be discussed within the sections to follow (Sections 1.5.3.2.1 to 1.5.3.2.6). With the goal of creating bimetallic silver/copper nanoparticles

(Chapter 4) certain constraints were put upon the synthesis conditions selected within this project. The motivations for producing copper bimetallics are explored in Chapter 4 and include the low cost and promising catalytic properties of such materials. In the synthesis of bimetallic nanoparticles both metals can either be added simultaneously, giving the potential for reaction and nucleation of both metals at the same time, or consecutively allowing one to nucleate first.[169–172] Since neither case allows for any post-synthetic size modification it can be argued that synthesis outcomes should be more successful, in terms of obtaining size controlled nanoparticles, if both monometallic equivalents lead to a high degree of size control independently (under the selected conditions). Additionally, for application in catalysis and spectroscopy, certain capping agents were thought to be undesirable and so the use of syntheses involving especially polymer capping agents was avoided, since they can inhibit catalysis or contain impurities that fluoresce (as seen in Chapter 3, Section 3.3).[129,173,174] In the case of silver/copper bimetallic particles, the copper was found to be more difficult to produce in small and monodisperse nanoparticle form. The production of uniform copper nanoparticles was therefore a key stage in our work.

1.5.3.2. Variation of synthetic parameters for furthering understanding of small copper nanoparticle synthesis

In order to investigate copper nanoparticle synthesis, in terms of parameters influencing the formation of small stable nanoparticles, the systematic variation of the synthesis conditions was investigated (Chapter 4). A survey of the current state of the art in the literature in this field, detailing the impact upon the particles produced and its relevance to our desired applications, is given in the sections below (Sections 1.5.3.2.1 to 1.5.3.2.4), along with a section (Section 1.5.3.2.5) detailing proposed reaction mechanisms gained through variation of two such parameters (reduction conditions, and temperature). Finally microwave and other alternate synthesis routes are discussed within Section 1.5.3.2.6.

1.5.3.2.1. The effect of variation of the reaction temperature upon copper nanoparticle synthesis

The nucleation and growth stages in nanoparticle synthesis are crucial in determining the properties of the particles obtained (Section 1.5.2). Theories such as classical nucleation theory, Ostwald ripening, and digestive ripening, are key in understanding such behaviour, yet the mechanism operating in any particular case is difficult to elucidate. Temperature variations within nanoparticle synthesis have a significant impact upon particle nucleation and growth, and upon the outcomes expected when each of the mechanisms above are operational. This might be the enhanced solubility of particles in hotter solutions, or the

impact upon kinetics of different stages of reaction. Examples of the exploration of reaction temperature as part of the synthesis of small copper nanoparticles are given within this section.

Mott *et al*. explored nanoparticle synthesis *via* reduction of a metal salt (copper(II)aceteylacetonate) at different reaction temperatures.[175] Variation of the ripening temperature allowed for the manipulation of the size and shape of the resulting nanoparticles. Two distinct temperature ranges were seen. With temperatures in the range of 150 to 190 °C giving a domain in which particle size could be varied for broadly spherical particles as given in Figure 1.11, whereas 190 to 210 °C gave a domain in which shaped particles dominated.

TEM for particles within the lower regime (150 to 190 °C) showed particles with a shape composed of coalesced spherical particles. This gave a variety of final shapes depending upon the number of particles coalesced, and so also resulted in variation in the particle size. Particles synthesised at 190 °C displayed a more spherical appearance as well as a higher degree of particle size dispersity. A roughly linear relation between particle size and the reaction temperature was reported, with particle size increasing as a function of reaction temperature (Figure 1.11). Some discrepancy was seen at higher temperatures, where the dispersion in the particle size was also seen to increase. The increase in particle size with reaction temperature was supported by TEM. The change in particle appearance seen from TEM imaging at temperatures above 190 °C suggested a change in the reaction mechanism had taken place. At these higher temperatures shape formation dominated. Particle size dispersity was larger in the shape dominated regime, this was in-line with the mechanism proposed in this domain as discussed in Section 1.5.3.2.5.2.

In summary for Mott *et al*. exploration of reaction temperature allowed for variation of the resulting particle size and shape. However, further optimisation of the synthesis would be required to reduce the degree of size dispersity in the particle sizes obtained.

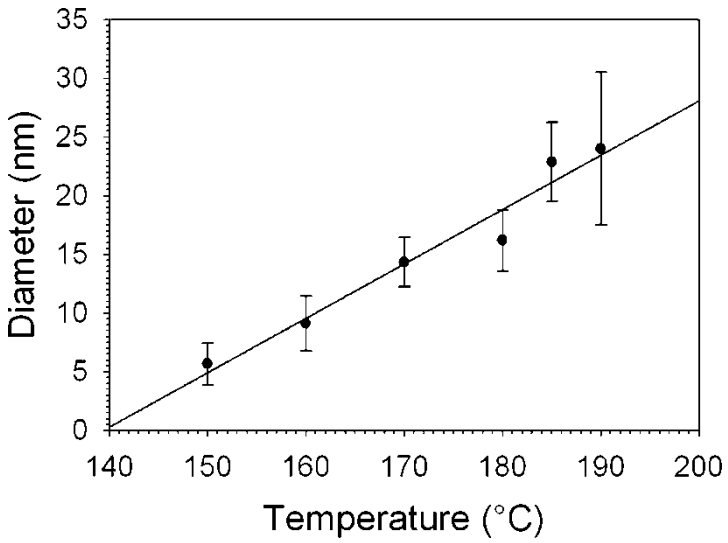

Figure 1.11. Reprinted with permission from (Mott, D., Galkowski, J., Wang, L., Luo, J. & Zhong, C. J. Synthesis of Size-Controlled and Shaped Copper Nanoparticles. Langmuir 23, 5740–5745 (2007)). Copyright (2007) American Chemical Society.

Although not their primary focus, Effenberger *et al.* briefly investigated the reaction temperature at which particle synthesis was conducted, or at least the metal salt copper(II)acetate was reduced by varying the reaction temperature in increments of 10 °C.[176] The colour of the nanoparticle solution and UV-vis spectroscopy confirmed that stable nanoparticles were not formed for reaction temperatures below 200 °C. They subsequently selected standardised preparation conditions using a temperature of 260 °C believing the reduction of the metal would be expected to take place efficiently at this temperature.

1.5.3.2.2. The effect of variation of the capping agent upon copper nanoparticle synthesis

The nature and concentration of the capping agent used in nanoparticle synthesis is known to be key to both the reproducibility and control over the properties of the particles produced.[177–180] In the case of easily oxidised copper metal, the stabilising effect of the capping agent might be considered even more crucial. Examples of the effect of varying the capping agent relevant to the synthesis of small copper nanoparticles are given below.

One key example is Effenberger *et al.* who investigated a number of mechanistic factors in the synthesis of copper nanoparticles, in particular the choice of capping agent used.[176] The synthesis they discussed was broadly similar to that used in this thesis (Chapter 4), based on a similar general reduction method and including in their screen the type of capping agents used here (oleylamine and oleic acid). Overall, however, they did not aim to produce small, monodisperse particles and wide particle size distributions were obtained.

Effenberger *et al.* synthesised copper nanoparticles by high temperature reduction of copper(II)acetate in a refluxing solution of diphenyl ether (approximately 260 °C) in the presence of a 1,2-octanediol reducing agent, and a capping agent.[176] The impact of changing and removing the capping agent was explored. The capping agents explored were 1,2-octanediol, oleic acid, and oleylamine.

For samples containing equimolar concentrations of oleic acid, and oleylamine, XRD showed the successful formation of copper(0), both in oxygen free conditions or after exposure to air for 24 hours. TEM imaging for particles synthesised in the presence of both capping agents and reducing agent, under the standardised conditions given above, gave large and polydisperse particles (approximately 30 to 200 nm). This might suggest further optimisation of the standardised preparation was required. For particles capped with only oleic acid, TEM showed a high degree of polydispersity (particle diameters range from a few to over 200 nm). Nanoparticles synthesised with only oleylamine capping agent displayed a high degree of agglomeration. Finally, for nanoparticles synthesised with both capping agents, in the absence of reducing agent, polydisperse hexagonal particles were seen.

It would therefore appear that some complementary effect was present for nanoparticle synthesised from the equimolar mixing of the two capping agents. This effect was not seen when either capping agent was used alone. The literature presents many examples of the use of these two capping agents together,[103,181–183] and there have been studies exploring the surface structure and stability of these dual capped nanoparticles.[184,185] Despite these various attempts, a succinct and unified understanding as to the origins of this effect does not currently exist. It has additionally been reported that changing the ratio of the two capping agents can result in controlled variation of particle sizes, which might be attributed to the reducing effect of oleylamine.[186]

Addition of 1,2-octanediol reducing agent did not significantly alter the particle size. Instead, the particle shape alone appeared to change. This may be indicative of 1,2-octanediol also acting as a capping or structure directing agent. As it has been suggested that capping agents can influence shape formation, with differing capping agents favouring growth on certain crystal facet this might explain the formation of hexagonal particles upon removal of 1,2-octanediol.[175,187]

As to the relative capping agent efficiency of oleylamine versus oleic acid for preventing particle agglomeration, this study may point to a slight enhancement for oleic acid which prevented agglomeration, but didn't control particle size effectively. However, given the

limited development of the standardised preparation used in this work along with the severity of polydispersity and agglomeration present throughout the samples, further studies would be required to confirm or further understand this observation.

Xiong *et al.* made very small copper nanoparticles with an average size below 2 nm.[188] The role was investigated for one species (L-ascorbic acid) capable of providing both reduction of the metal precursor, as well as acting as a capping agent for the nanoparticles formed. UV-vis spectroscopy and TEM imaging were used to investigate the impact of varying the concentration of the reducing and capping agent, L-ascorbic acid. All UV-vis spectra displayed a strong band centred around 330 nm assigned to oxidised L-ascorbic acid. This might be linked to reduction of the copper salt. A second peak centred around 570 nm was seen, and attributed to absorbance from the copper nanoparticles. As the capping and reducing agent concentration was increased the second peak broadened and the wavelength of the peak increased. This might suggest that larger particles were formed by increasing the concentration of L-ascorbic acid. Larger quantities of L-ascorbic acid might be thought to provide faster reduction, resulting in a faster particle nucleation. This then provides more time for particle growth to occur, leading to larger particle sizes. TEM imaging showed small, spherical and monodisperse particles of sizes below 2 nm. Within errors no significant change in particle size was seen as the concentration of L-ascorbic acid was varied. Hence no clear indication of the impact, of varying the concentration of the joint capping and reducing agent, was seen.

The stability of the system was particularly important, as it allows some assessment of the capping ability of the L-ascorbic acid. The physical appearance of the particle solution was used to access stability. No sedimentation was seen for particles stored for up to 2 months (particle agglomeration could lead to sedimentation). Precipitate was seen after initial nanoparticle formation, the precipitate was water soluble upon sonication. The precipitate may be due to the formation of larger heavier particles. It was unclear whether such large material was included in TEM imaging conducted. The capping functionality of the molecule also appeared to be key, and seemed to be interlinked with the water solvent system. It was therefore unclear if L-ascorbic acid would provide as strong a reducing and capping effect in other solvent systems.

Another example of relevance showed control particle size from 3.6 ± 0.8 nm to 10.7 ± 0.7 nm, by varying the molar ratio of copper precursor; capping agent (between 0.08 and 0.6).[189] Particle size was seen to increase as a function of increasing capping agent

concentration. This is in contrast to the established idea that larger capping agent concentrations are required to allow formation of very small nanoparticles, due to their inherently larger surface areas meaning that a greater degree of stabilisation is required. The authors did not provide any argument as to the nature of this unexpected result. However, trioctylamine is present within the preparation, a species which is capable as acting as a capping agent. It is therefore possible that when the oleic acid concentration is lowered significantly trioctlyamine becomes the dominant capping agent. Given that the amine would be expected to give differing binding behaviour greater stabilisation may be provided resulting in the smaller particle size.

1.5.3.2.3. Redox effects: The effect of variation of the reducing agent upon copper nanoparticle synthesis, focusing upon the reduction of copper metal and the stability of synthesised nanoparticles to oxidation

Thermal reductions are commonly used in nanoparticle synthesis, and often rely upon the use of elevated reaction temperatures, to achieve reduction of the metal salt (to the metal oxidation state).[107,108,110] In such cases the solvent may act as the reducing agent, for instance conventional polyol synthesis, where the alcohol functional groups of the solvent act as a weak reducing agent.[129] Reducing, and coordinating capping agents such as oleylamine, which have a weak reducing effect, can also be used.[186] However, reduction by these weak reducing agents is often slow, and so can lead to polydispersity in the particles created. Hence addition of stronger reducing agents can be used to quickly facilitate reduction of the metal salt. This leads to fast reduction and subsequent burst nucleation (*i.e*. all nucleation events take place together), which often results in a more monodisperse particle distribution, as well as access to smaller particle sizes.[190] The effect of varying the concentration and nature of the reducing agent was explored for examples of relevance to the copper nanoparticle synthesis within this work. The efficient reduction of the copper metal, and the stability of the synthesized nanoparticle, with respect to decomposition are identified as key factors and explored within this section.

Xiong *et al.* utilised a simple methodology at 80 °C with the reduction of copper(II)chloride dihydrate in water using L-ascorbic acid as both the capping and reducing agent.[188] Water was used as a supposedly green solvent, however the synthesis of stable copper nanoparticles in the presence of water would arguably be expected to be challenging due to the ease of oxidation in such a system, especially as there is no indication the water was degassed before use. Therefore, very strong metal reduction and subsequent stabilisation *via* the capping agent species would be required. As discussed above, L-ascorbic

acid was used as both the reducing agent and the capping agent, and within error no significant change in particle size was seen as the concentration of L-asborbic acid was varied. In this particular case there was therefore no clear indication of the impact of varying the concentration of the reducing agent, although the reaction rates of processes in this example may be complicated by the dual role of ascorbic acid as both capping and reducing agent.

A mechanism for the reduction by L-ascorbic acid was put forward in which it is oxidised to a dehydrated form. The reduction potential for the reduction of the dehydrated form to ascorbic acid is +0.060 V versus SCE. The reduction potential for copper(II) to copper(0) is 0.340 V versus SCE, both are two electron processes and so the overall standard potential is +0.280 V, confirming its capacity to act as a reducing agent in this reaction. Whether the role of L-ascorbic acid is dependent upon the water solvent system was unclear, and unfortunately being very hydrophobic, it is difficult to draw comparisons with the long chain amine and acid systems above and in the present work.

Yin *et al*. also reported an assessment of the stability of small monodisperse copper particles with an oxide shell.[189] After washing particles under inert gas, the washed particles dispersed in hexane were simply exposed to air and the solutions colour changed from burgundy to green. No additional oxidative treatment took place. Given the aim of the authors to make particles with a copper oxide shell, it was important to establish that oxidation occurred only at the metal surface. Reduction of the metal salt to the zero-valent copper nanoparticles, should have occurred during the preparation (conducted in inert conditions to exclude air or other oxidative media). As indicated in Figure 1.10, re-oxidation during nanoparticle synthesis before particles are formed can inhibit their formation or result in dissolution of the oxidised copper. The subsequent oxidation of the surface to give a copper(0) nanoparticle core to form a copper(I)oxide and/or copper(II)oxide shell should therefore occur only after the nanoparticle synthesis. To confirm such a process had taken place a number of characterisation techniques were employed. Firstly XRD showed the evolution of the cuprite (copper(I)oxide) type structure, for material exposed to air post synthesis. For freshly synthesised material phases seen were associated with copper metal, and only small amounts of the copper oxide (110) phase were seen. The intensity of the oxide phases were seen to grow with air exposure as expected. The phases associated with the copper metal core (Cu(110), Cu(200), Cu(220)) were still detected, and only small changes in the intensity of these peaks were seen. TEM imaging also gave evidence of oxide shell formation, with particles showing a dark core and a paler coloured shell. This was attributed to the copper nanoparticles and oxide shell respectively. Lattice plane distances, and the

presence of twinning, in HREM imaging, also gave an indication of an fcc copper(I)oxide structure. Both UV-vis spectroscopy and XPS, which is inherently surface sensitive, gave further evidence of a copper oxide surface structure. XPS gave an approximation of the thickness of the copper oxide surface layer as 0.5 nm. The analysis undertaken allowed some level of confidence that the material produced was composed of copper nanoparticles, with oxidised material present only at the surface. Such oxidation was likely to have taken place after the completion of the nanoparticle synthesis. There was therefore sufficient evidence of a copper nanoparticle core and oxidation at the surface only.

The work described previously (Section 1.5.3.2.1) by Mott *et al.* also included an assessment of oxidative stability.[175] To assess the particle stability of the as synthesised copper nanoparticles the solutions were left open to air for several weeks. No change in colouration was observed (although it is not clear if this experiment was performed on much larger nanoparticles where the surface/bulk ratio is much lower). Oxidation of the metal ions to either the copper(I) or copper(II) oxidation state could either result in an oxide layer growing or result in decomposition of the nanoparticle by dissolution of metal ions. Either would have given rise to a colour change to a green or blue nanoparticle solution, and a shift in the UV-vis and neither was observed, although it should be noted that the dark colours of nanoparticle solutions can disguise lower concentrations of the soluble oxidised copper ions.

Nanoparticle oxidation was also investigated for the case of the Cu_8 cluster prepared by Wei *et al.*.[191] XP spectra showed two bands, assigned to the $2p_{3/2}$ and $2p_{1/2}$ of copper(0). The authors noted the absence of copper(II) groups, but also the close proximity (approximately 0.1 eV) of copper(0) to copper(I) bands. The authors therefore suggested the likelihood of charge transfer to the capping agent, facilitating an oxidation state between 0 and 1. XP spectra appeared to be indicative of metal reduction having occurred. The strong binding of the thiolate capping agent, would be expected to provide sufficient stabilisation, against oxidation and subsequent decomposition and the small size of these clusters renders them somewhat more molecular in nature than the larger nanoparticles mainly under consideration.

Effenberger *et al.* used XRD to confirm the formation of crystalline phases associated with copper(0) for the case of their standard preparation,[176] which used equimolar concentrations of oleylamine and oleic acid. This was seen for a sample maintained in oxygen free conditions, as well as for that exposed to air for 24 hours. This indicated at least short term stability of the zero-valent metal nanoparticle, since XRD is only sensitive to crystalline

components of a sufficient size to be seen by diffraction, this does not exclude the possibility of a thin or amorphous oxide layer growing over the surface of the particle.

Crystal phases associated with copper(0) were detected by XRD for all particles synthesised in the presence of a capping agent. This included material synthesised in the absence of a reducing agent, indicating full reduction to zero valent oxidation state could be achieved by thermal reduction alone, where one of the capping agents must play the role of reducing agent. In the absence of capping agent, two phases were seen of which 5% was attributed to copper(0) and 95% to copper(II)oxide. For particles in oxygen free conditions only copper(0) phases were seen by XRD, suggesting that nanoparticles were formed, but were oxidised in air as shown in Figure 1.10.

1.5.3.2.4. The effect of variation of the reaction time upon copper nanoparticle synthesis

Ripening time is the term given for the period in which the reduced metal is held at high temperature (sometimes referred to as aging) for particles to grow or ripening to occur. Variation of the ripening time can allow insights into the reaction mechanism. For example variation from short to longer ripening times may allow elucidation of whether the particle growth follows an Ostwald or digestive ripening type mechanism (Section 1.5.2). No examples of ripening time variation in systems of direct relevance to the synthetic approach employed within this report were found.

1.5.3.2.5. Mechanistic studies

Examples of particular interest to increasing mechanistic understanding of the synthesis of small copper nanoparticles are detailed within this section.

1.5.3.2.5.1. Reduction mechanisms

The mechanism of reduction, or more specifically the oxidation of the reducing agent, proposed by Xiong *et al*. is given in Figure 1.12.[188] The transformation of L-ascorbic acid through to dehydroascorbic acid *via* the loss of $2H^+$ was expected to facilitate the reduction of copper(II) to copper(0) (both are two electron processes).

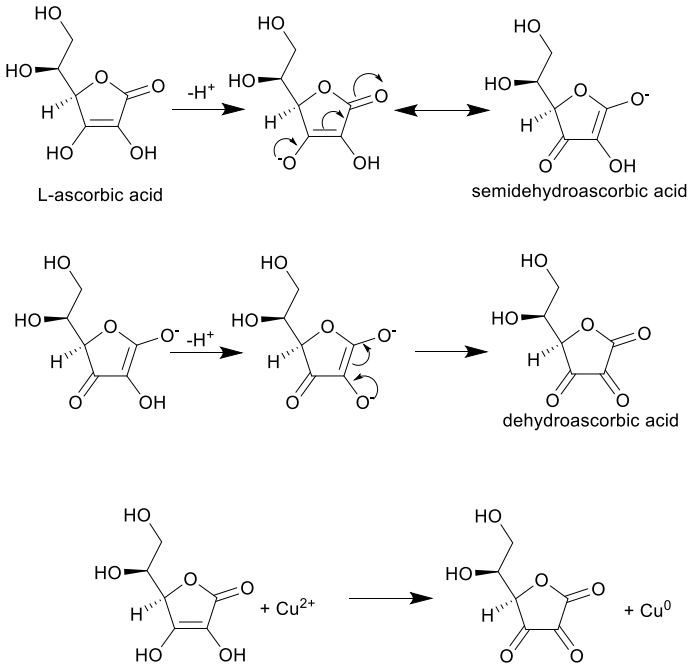

Figure 1.12. Reaction scheme adapted from that proposed by Xiong et al.,[188] *for the reduction of copper(II) to copper(0), by L-ascorbic acid.*

For assessment of the capping ability of the L-ascorbic acid, two possible contributing factors were put forward. Firstly, it was suggested that interaction between the lone pairs of the electronegative oxygen groups of the ascorbic acid and the copper ions sp orbitals took place before reduction existed. It was suggested that this interaction facilitated subsequent capping, by locating the resultant copper atoms in close proximity. The second contribution identified was that the dehydroascorbic acid oxidation product rapidly undergoes hydrolysis to form a polyhydroxyl species which likely serves as an effective capping matrix for the nanoparticles formed. FTIR analysis agreed with this type of hydrolysed structure being present on the surface of the nanoparticles.

1.5.3.2.5.2. Mechanistic interpretation of temperature effects on particle size and shape

Mott *et al*. considered the mechanisms giving rise to the size (lower temperatures) and shape (higher temperature) dominated regions they had reported.[175] Firstly the change in particle appearance across the size dominated regime was examined, and it was noted that larger particles contained possible evidence for their origin being a number of smaller particles that had coalesced. It was proposed that higher reaction temperatures promoted the desorption of the capping agent. This may have led to the formation of the larger and more spherical particles seen for the 190 °C ripening temperature, since the desorption of capping agent would allow access of other particles or of metal atoms to the surface. They argue that

capping agent desorption is a requirement for particle growth.[89,192] If such effects are not uniform throughout the sample or because the aggregation of different numbers of particles may result in different sizes then this might also explain the large degree of size dispersity seen at 190 °C, although beyond noting the much greater dispersity is observed this is not discussed by the authors.

The authors went on to introduce the idea of surface melting of the copper nanoparticle, and linked it as being significant to this proposed mechanism. They suggest, based on depression in the bulk melting point of nanoparticles on going to smaller sizes, that surface melting of the copper should also occur more readily for smaller particles, which aids coalescence. It was the authors' view that in their preparation surface melting of smaller copper particles also contributed to the particle coalescence observed, although specific evidence for this is not provided and other than by analogy to the melting point of whole nanoparticle it was not clear whether surface melting would occur for particles of this size under the preparation conditions used.

For nanoparticles synthesised in the temperature range in which shaped particles dominated, the authors noted the absence of coalescence in the TEM imaging. This indicated a differing mechanism, to that seen in the lower temperature (150-190 °C) domain. The similarity in the shape formation exhibited to that in the work of Pileni *et al*. was noted.[193] They proposed that shaped precursors formed, and that preferential adsorption of the capping agents occurred on the nanocrystal facets. Given that two capping agents were used in the preparation, it was plausible that differing crystal facets were favoured by the two capping agents. The authors proposed that the differing shapes seen were attributed to differing seed precursors. Preferential adsorption of the two capping agents to these varying seeds lead to a variety of different shaped nanoparticles. The particle appearance fitted with a mechanism based upon inter-particle coalescence and capping agent removal.

1.5.3.2.6. Microwave synthesis and other alternatives

Small copper nanoparticles have been synthesised using microwave synthesis. Kawasaki *et al*.,[194] is one such example.[195–197] This synthesis claimed to offer the advantage of nanoparticle synthesis without the use of an organic capping agent. Capping agents can be detrimental to certain applications, and difficulty of removal can also be an issue. So synthesis in the absence of capping agent is seen by some as being highly advantageous. However, stabilising the recently reduced nanoparticles, and maintaining the zero-valent oxidation state, as well as preventing particle aggregation can be a significant challenge in

the absence of a capping agent. In this case 2.3 ± 0.25 nm particles were synthesized in ethylene glycol, and TEM imaging showed the monodispersity of the particles, although some evidence of particle aggregation was seen. However, the authors note the stability of the particles is likely due to the formation of polyethylene glycol by ethoxylation of the ethylene glycol during the microwave reaction, so in practice it is likely the particles are polymer capped or polymer embedded and so probably not suited to applications in catalysis. In addition, microwave-based synthesis is not readily scalable, requires specialist equipment, and can suffer from difficulties in terms of reproducibly. Hence despite the excellent size and polydispersity of the nanoparticles synthesised by Kawasaki *et al.*,[194] we do not believe microwave synthesis to be suitable for the copper nanoparticle applications intended in this work.

Similarly other techniques such as micro-emulsion and electrochemical methods have produced promising small copper nanoparticles with the desired properties such as stability and monodispersity.[198,199] However, such techniques are unlikely to be compatible with catalytic applications, and can be difficult to generate sufficient quantities of sample even for small scale testing.

1.5.3.3. Summary of the overview of the state of the art

To summarise, a number of differing methods for the synthesis of small stable copper nanoparticles have been explored. Mechanistic interpretation as well as evaluation of changing experimental parameters such as capping agent, or ripening temperature has been discussed. This has informed the starting point of the presently reported synthesis (drawing especially on work by Mott *et al*.).[175]

Despite the obvious advances in the field, significant scope for furthering the understanding of the targeted synthesis of small stable copper nanoparticles still exists and is urgently needed for the proposed application of such materials in catalysis and spectroscopic studies of catalysts. This is the starting point and aim of the work conducted within this chapter.

1.6. Catalytic systems and metals of interest to this study

As detailed in Sections 1.1 to 1.5 it was the aim of this work to synthesise nanoparticles for use as model heterogeneous catalytic systems. TIR Raman would then allow for *in situ* surface sensitive characterisation of these catalytic systems. This aimed to elucidate greater mechanistic understanding for heterogeneous catalysis. Therefore, the careful selection of heterogeneous catalytic systems was required. Ethylene epoxidation was chosen as it represented a system in which a number of fundamental mechanistic questions remained,

particularly as to the nature of species at the catalyst surface, which TIR Raman is potentially ideally suited to answer. The system also included scope for the improvement of the model catalysts used, for example many studies have relied on traditional incipient wetness catalysts from metal nitrates where particle size and composition may be poorly controlled. Studies attempting to understand the interaction of copper and silver in bimetallic catalysts have relied on an inhomogeneous commercial (Sigma Aldrich) silver-copper powder.[200] The synthetic goals of this thesis in producing small copper and copper bimetallic structures took this system as an inspiration.

Furthermore, it was important to demonstrate that some of the nanoparticle systems made could be used directly in catalysis. The resulting catalysts were carefully tuned to display properties such as unusual and high activities or selectivities (one key example being that of furfural hydrogenation). The state of the art within these areas is discussed in the sections that follow (Section 1.6.1 onwards).

1.6.1. Ethylene epoxidation, catalysts and mechanisms

Epoxidation is the process in which partial oxidation of an alkene to an epoxide takes place. A scheme for the epoxidation of ethylene to ethylene oxide is shown in Figure 1.13. This example represents the simplest case, and one in which no allylic hydrogens are present. Ethylene oxide has a wide range of potential applications, producing an annual turnover of $18 billion.[201] For example one application of ethylene oxide is as an intermediate in the creation of ethylene glycol. There is a high demand for ethylene glycol due to its use as a component in antifreeze, polyester, surfactants and detergents.[202–204] Industrially the epoxidation of ethylene to ethylene oxide is typically performed using a silver catalyst on an α-alumina support; the process taking place in the presence of an oxygen gas feed. It is estimated that a 1% increase in selectivity in ethylene epoxidation would generate around $180 million annually.[201]

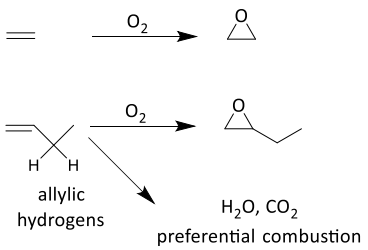

Figure 1.13. Diagram to show epoxidation of ethylene and a higher olefin (but-1-ene). The latter shows the unselective preferential combustion pathway (preferential combustion of the allylic hydrogens).

As shown in Figure 1.13, the reaction becomes more complex in the presence of allylic hydrogens, where two different selectivity pathways are possible. In this case, allylic hydrogens can lead to aldehyde formation and so to preferential combustion. Preferential combustion gives the formation of water and carbon dioxide (which is thermodynamically preferred). This means the corresponding epoxide is not formed, or formed with significantly lower selectivity. Therefore a key requirement of the catalyst is selectivity to produce the epoxide product. Key parameters to increasing such selectivity include understanding the reaction mechanism as well as the role of promoters used (typically chlorine and caesium).

1.6.1.1. Ethylene epoxidation mechanisms

Initially it was hypothesised that a special kind of adsorbed oxygen might be present. This came from the work of Kilty *et al.*,[205] who were one of the first to try to attempt to predict the mechanism for ethylene epoxidation. They hypothesised that there were two types of oxygen present, atomic oxygen (O) and charged molecular oxygen (O_2^-). They believed that the molecular oxygen was chemisorbed onto the surface of the silver catalysts. They believed this to be responsible for the selective epoxide forming route, while the atomic oxygen gave rise to the unselective preferential combustion route. Under these conditions the authors concluded that the maximum achievable selectivity would be 86%.

However, a decade later groups began to achieve selectivities above 86%. Furthermore Grant and Lambert used temperature programmed desorption (TPD) to remove the molecular oxygen from a silver(111) surface.[206] This experiment showed no influence upon the production of ethylene oxide. The reaction had to be occurring *via* the atomically absorbed oxygen. They believed that two types of adsorbed oxygen were present. One form was low valence charged and electrophilic, and gave rise to the selective route. The other form was electronegative, with a high valency and also charged. They believed the second form of oxygen abstracted hydrogen (due to its electronegativity) and so gave rise to the preferential combustion.

However, in 2002 Linic and Barteau postulated a very different mechanism.[207] They believed that the nature of the absorbed oxygen on the silver surface, was not the factor determining the selectivity. Instead, based upon DFT calculations, they argued an intermediate oxametallacycle existed. From this intermediate two routes were possible. These two routes were predicted to be similar in energy, and gave rise to the selective and unselective products. The scheme for these two routes is shown below in Figure 1.14. It is noted that at the time there was debate as to whether the OME (oxametallacycle bound to one silver with

a 4 membered ring) or OMME (oxametallacycle bound to two silver with a 5 membered ring) existed, hence both are shown in the scheme.

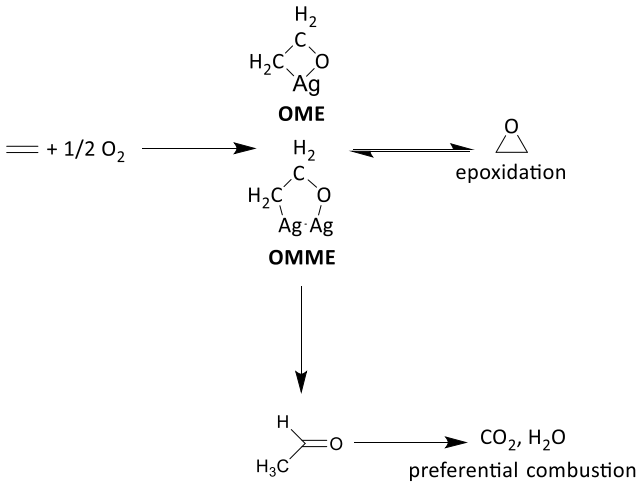

Figure 1.14. Reaction Scheme for reaction mechanism for ethylene epoxidation as proposed by Linic and Barteau in 2002.[207] OME and OMME represent the two differing oxametallacycles predicted.

As mentioned previously, an increase in selectivity, to the epoxide, was seen in the presence of chlorine and caesium promoters. Linic and Barteau used the proposed mechanism to explain this enhanced selectivity.[207] They believed that chlorine acted through the surface to stabilise the selective intermediate. They proposed that caesium acted through space in much the same way.

However, experimental work by Waugh and Hauge (2005) contradicted these findings.[208,209] Firstly, they found that the ethylene oxide selectivity was a function of the silver-oxygen bond strength (for a silver catalyst). A weaker silver-oxygen bond was seen to be more selective. Their explanation of the chlorine and caesium promoter effect, was that chlorine promoted the weakening of this silver-oxygen bond. This then led to increased ethylene oxide selectivity. They proposed that caesium occupied the sites in which the strongest silver-oxygen bonds were formed, this prevented them from forming and aided selectivity.

The work of Waugh and Hauge in 2010 furthered these observations by proposing an alternate epoxidation mechanism.[210] This mechanism suggested that an oxametallacycle was not formed. Instead they believed a different common intermediate was created. This intermediate is shown in the reaction scheme which is given in Figure 1.15. It was suggested that upon intermediate formation two pathways were available. The bond could either undergo silver-oxygen breaking to give the desired epoxide product, or hydrogen abstraction could occur to give preferential combustion. A weak silver-oxygen bond favoured the prior, and a strong bond the latter. The selectivity enhancement of the promoting species was

rationalised in that chlorine weakened the silver-oxygen bond and so increased the epoxide selectivity. Caesium was held on the stepped silver surface, and so prevented strong silver-oxygen bonds from forming. This was in agreement with the group's previous theory.

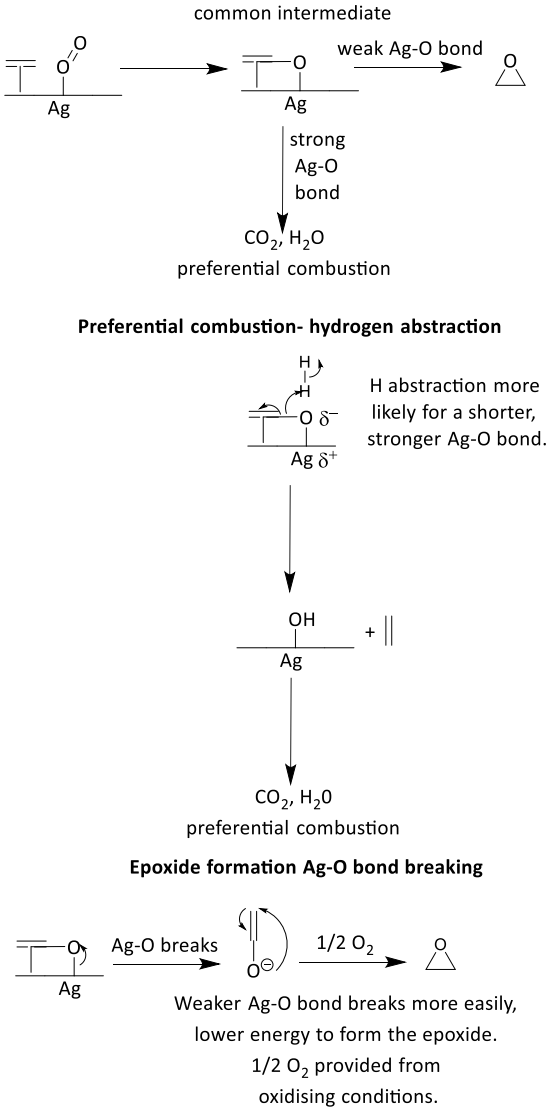

Figure 1.15. Reaction scheme for reaction mechanism for ethylene epoxidation as proposed by Waugh and Hague 2010.[210] Scheme details one common intermediate, and two paths to selective and unselective routes to ethylene epoxidation.

It should be noted that not all of the literature is in agreement with this explanation. For example the review by Bukhtiyarov and Knop-Gericke,[211] published in 2011, postulated a largely similar mechanism, but with some details differing. The mechanism given for ethylene epoxidation over a silver catalyst followed the scheme given in Figure 1.16. Their mechanistic understanding was underpinned by the belief that two types of oxygen were present. These were electrophilic and nucleophilic oxygen, in agreement with much older mechanistic theories. As can be seen in Figure 1.16, they believed that the electrophilic oxygen was

required to form the cyclic ethylene oxide. Furthermore they stated that the nucleophilic oxygen led to preferential combustion. They also proposed that under reaction conditions further oxygen species could be formed, and it was these which lead to acetaldehyde formation. This then gave preferential combustion. This mechanism was proposed for an unsupported silver catalyst. For a supported silver catalyst, for example on alumina as is typical for this reaction, the authors believed the mechanism would be altered. The proposed mechanism changed only by the electrophilic oxygen delivery method, which was *via* the defect phases on the silver. The authors also drew attention to the ability of the support to prevent sintering.

The explanation of the chlorine promoter effect was again based upon its electronegativity (in accordance with Waugh and Hague).[210] However, unlike Waugh and Hague, Bukhtiyarov and Knop-Gericke felt that the electronegativity seen instead led to an increase in the heat of ethylene absorption, and so in turn to an increase in the amount of ethylene absorbed onto the silver catalyst. This theory was based upon both TPD data and the literature at that time.[212,213]

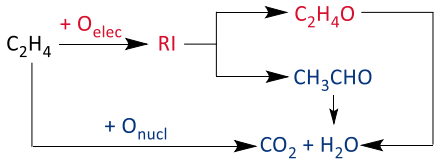

Figure 1.16. Proposed reaction mechanism for ethylene epoxidation on a silver catalyst. Adapted from Bukhtiyarov and Knop-Gericke.[211]

1.6.1.1.1. Summary of mechanisms for ethylene epoxidation

It can be seen that there is still much debate as to the reaction mechanism for ethylene epoxidation and as to the role of the promoter species. This question is of importance due to the industrial significance of ethylene oxide and ethylene glycol. Ethylene epoxidation, is therefore, a system of considerable interest and one that we would like to study with TIR Raman. The capabilities of TIR Raman (see Section 1.4) make it ideally suited to answering such questions of surface reactivity, and intermediate detection.

1.6.1.2. Ethylene epoxidation catalysts: traditional and alloy type catalysts, for ethylene epoxidation

Typical ethylene epoxidation catalysts comprise of silver supported on α-alumina.[214–217] However, as mechanistic knowledge increased so did the optimisation of catalyst formulations. One successful technique which has been used, at lab scale, is to employ an silver-copper bimetallic alloy catalyst. In 2004 Linic *et al*..[218] varied the catalyst composition

in order to try to improve its selectivity. The work was underpinned and relied upon the proposed oxametallacycle mechanism, along with earlier studies of the transition state energies,[219] kinetic isotope effects,[220] and microkinetics.[221] DFT computational modelling, was combined with combinational screening in order to calculate the binding energy, and geometry for a series of the silver-metal alloys. Only small amounts of the alloy metal were added. This was with the intention that under such conditions, the surface chemistry and reaction mechanism would not change. The catalysts screened by DFT were then classified, as either good or bad. Catalysts were good if the barrier to acetaldehyde, from which it is postulated that preferential combustion occurs, was higher than that to ethylene oxide. The best catalysts were then synthesised and supported to allow for catalytic testing. From this approach a silver/copper blend catalyst was created, which the authors supported on an alumina monolith, using a wet impregnation. It should be noted that the authors were not the first to use copper as an epoxidation catalyst. Earlier work by Cowell *et al.,*[222] and Santra *et al*., had explored copper as a catalyst for styrene epoxidation and suggested that in some ways copper might be considered a more effective catalyst.[223] They had noted both the lower temperature required by the copper catalyst for epoxidation of styrene, as well as the lower quantities of combustion products created. Some precedent, therefore, existed for the use of this metal, and it would be of particular interest to understand the effect of combining the two metals.

Catalytic testing gave some early indications of improved selectivity and activity. However, it should be noted that two catalyst batches were made (batch A and batch B). The batches were described as being made from differing “lots” of silver, copper, and alumina, presumably referring to differing batches of material from the same supplier. The catalytic activity of the base silver catalysts made for each batch was seen to differ. Furthermore the copper loadings used for batches A and B were not the same. This made it difficult to directly compare catalytic activity or selectivity between the two batches. However, in general an increase in catalytic activity was seen for the silver/copper catalyst compared to the silver alone. Proposed trends in ethylene oxide selectivity, may have been less significant in light of such errors. Selectivity results were normalised, by comparing the measured selectivity to that of the bulk catalyst (the batch used and that compared against was not specified). The authors deduced that the maximum selectivity of the silver/copper alloy was around 1.5 higher than that of the silver catalyst. This was for a composition, in terms of moles of copper per mole of silver, of approximately 0.8%. However, this was very much a preliminary result, as only one set of conditions for temperature and feed pressure were used. As the copper

content was increased from zero, a rapid increase in selectivity was observed. However, the rate of this effect decreased for copper contents above approximately 0.25% copper mole per mole silver. Therefore, despite 0.8% of copper giving the highest outright selectivity, it may not have represented a region of best rate of change of the selectivity.

Finally, the authors recorded post reaction XP spectra for a selection of the catalysts. The copper concentration on the top few layers of the surface, was significantly higher than expected from the bulk copper content. It was postulated that copper migrates to the surface, due to its higher affinity to oxygen than the silver. It should be noted that the conditions the XPS was performed under were not described. If the sample was exposed to air, oxidation of the copper may have occurred. Therefore the sample may not be representative of the catalyst under reaction conditions.

In conclusion, this paper provides some preliminary evidence, that silver/copper bimetallic catalysts may increase catalyst selectivity when compared to traditional silver only catalyst blends. However, error analysis, particularly related to variation of the properties of the two batches of catalyst synthesised, as well as further mechanistic studies would also enhance the evidence presented. Furthermore, the work of course relies upon the formation of an oxametallacycle and the corresponding reaction mechanism. The DFT calculations and the selection of suitable alloys were determined from this assumption. As discussed previously there is still much debate as to whether this intermediate exists. This does, therefore, place some doubt upon the validity of the corresponding mechanism, and so upon the results presented. DFT calculations using an alternate reaction mechanisms might have yielded differing results and lead to the optimised selection of a different catalyst blend.

1.6.1.3. Further exploration of alloy type catalysts, for ethylene epoxidation

In 2005 Jankowiak *et al*.,[224] expanded upon the work of Linic *et al*..[218] The authors undertook an in-depth study of the catalysts proposed by Linic *et al*..[218] Systematic variation of the reaction conditions took place, in order to allow determination of the RDS. The kinetics of the reaction were studied, using thermal conductivity detector (TCD) gas chromatography. This lead to determination of the reaction rates and order. Reaction feed and temperature were also varied, with the intention of elucidating further mechanistic insight. Finally, simultaneous feedstock variation allowed for the production of a 3-dimensional selectivity contour map.

1.6.1.3.1. Probing of reaction mechanism and Rate Determining Step (RDS)

It was proposed that the RDS varied as the catalytic conditions were altered. The authors suggested two possibilities for the RDS. Firstly that the RDS was the dissociative adsorption of the oxygen. Secondly that the RDS was the surface mediated reaction of ethylene and oxygen to form the oxametallacycle. The equations for these two steps are shown in Equation 1.2. For which * represents unoccupied surface sites. A gas phase species is depicted by (g), and by (a) a species which has been adsorbed onto the catalyst surface.

$$O_2(g) + 2* \leftrightharpoons 2O(a)$$
$$C_2H_4(a) + O(a) \rightleftharpoons CH_2CH_2O(a) + * \qquad \textit{Equation } 1.2$$

The authors aimed to observe a change in the RDS. This was targeted by systematically varying the feed conditions whilst monitoring the reaction conversion, selectivity and rate.

1.6.1.3.1.1. Variation of copper content, and reaction feedstock for the monometallic and alloy catalysts

Catalysts with varying copper contents were prepared by wet impregnation. The following molar percentages of copper where used: 0.1%, 0.2%, 0.5% and 1%. Two batches of catalyst were prepared. It can be seen that fewer copper concentrations were investigated than by Linic *et al*.,[218] but a larger range of values were targeted. Again, significant batch variation was seen. The origin and impact of such variation upon the results obtained was not discussed. Each catalyst blend was held in the reactor for 24 hours (a process referred to as lining out). All samples were held under the same conditions. This allowed for stabilisation of the catalyst activity and selectivity. The reaction conditions were then altered, with the oxygen and ethylene gas feed content varied. The effect upon the catalyst activity and selectivity was monitored. The alloys outperformed the silver only catalyst, in terms of activity and selectivity, under all reaction conditions. Variation of the ethylene concentration did not significantly affect the reaction rate, whereas an increase in the oxygen content gave an increased the reaction rate.

Reaction orders were calculated, for ethylene and oxygen, using power law kinetics. This was done with either the oxygen or ethylene content fixed (to 10%), while the other feed was varied from 10 – 60% and the temperatures varied to 500, 520, and 540 K. The corresponding reaction orders seen were zero or negative order, with respect to ethylene. The reaction was positive order with respect to oxygen. This indicated a dependence upon the oxygen feed content only. This was in agreement with the activity and selectivity data given.

1.6.1.3.2. Determination of reaction order, from variation of reaction feedstock and temperature

Reaction orders for oxygen and ethylene were then calculated. Calculations used data for ethylene consumption, and ethylene oxide and carbon dioxide formation. The authors concluded that under ethylene rich feedstocks, the RDS was not dependent upon ethylene. The RDS was, therefore, the dissociative adsorption of oxygen. Under oxygen rich feedstocks the RDS was seen to be dependent upon oxygen. This meant the RDS could be either of the two steps. In order to determine which step was rate determining, the ethylene reaction order was measured under oxygen rich conditions. Conditions of 10% to 30% ethylene and 60% oxygen were used. It was concluded that the RDS was influenced by the feed composition. Reaction orders for ethylene oxide and carbon dioxide were then measured, under both ethylene and oxygen rich feed conditions. This was first conducted for the silver only catalyst. This allowed deduction of the effect of changing the feedstock composition upon the product distribution. At high ethylene contents the ethylene oxide production went down. This corresponded to the reaction order decreasing from 0.2 to -0.2. The reaction order also decreased as the reaction temperature was reduced. Correspondingly, increasing the ethylene content was found to lead to a decrease in catalytic activity.

Carbon dioxide formation showed a negative dependence on the ethylene feedstock. Reaction orders went from -0.2 to -0.4 as the ethylene content was increased. Again some differences were seen between the behaviour of the two catalyst batches. Qualitative trends were reproduced, but some variation was seen between the values received for the two batches. The discrepancy seen was small.

Overall increasing the ethylene concentration lead to an increase in selectivity for the silver catalyst. This was at the expense of the catalyst's activity. For oxygen rich feedstocks ethylene oxide reaction orders ranged from 0.4 to 0.7 and carbon dioxide from 0.2 to 0.3. This indicated that both selectivity and activity could be enhanced, by increasing the oxygen concentration. Again some differences in these values were seen between the two catalyst batches. The magnitude of these differences was not excessively large. The authors stated that this result was in agreement with the work of Monnier *et al*.,[225] in which an increased olefin concentration gave increased selectivity in butadiene epoxidation. However, Monnier *et al*. stated that the selectivity trends seen for butadiene epoxidation,[225] were the opposite of those seen for the reaction of ethylene to ethylene oxide.[226,227] A number of notable differences exist between the two reactions. These include the alternate reaction pathway

seen for ethylene epoxidation, which gives preferential combustion forming carbon dioxide and water. Such a pathway was not seen for the butadiene reaction. For ethylene epoxidation this causes the ethylene feed concentration to be inversely proportional to the ethylene oxide concentration. Therefore selectivity results between the two systems may not be not comparable.

The effect of the alloy catalyst upon the ethylene oxide selectivity was examined by fixing the ethylene conversion for the silver and alloy catalysts. Differing feed compositions were then used. For all of the alloy catalysts high ethylene contents gave increased selectivity. This was in agreement with the data obtained for the silver catalyst. The alloy catalyst consistently gave enhanced selectivity compared to the silver catalyst. Clearly it can be seen that positive results have been obtained by mixing silver and copper as an ethylene epoxidation catalyst, yet the detailed understanding of the surface or adsorbate structure has remained elusive. This is the reason copper and copper silver nanoparticles, that would give a high degree of control of size and composition and in due course be amenable to in situ spectroscopic investigations, have been a focus of this project.

1.6.1.4. Mechanistic insights into copper as an epoxidation catalyst: DFT modelling, and in situ XPS studies of the nature of the copper-silver alloy catalyst surface

Work by Piccinin *et al.* went on to explore the surface chemistry of copper and silver alloy catalysts for epoxidation under more realistic reactions conditions (*i.e.* not UHV).[200] In parallel, DFT modelling allowed for surface phase diagrams to be produced and an initial understanding of the composition of the catalyst surface. *In situ* XPS was then used during catalytic testing in order to allow for testing of the theoretical predictions. This allowed for the on-line monitoring of species present at the catalyst surface. Offline TEM and XRD analysis were also used allowing for deduction of the particle appearance and crystallinity of the used catalyst, although the sample used was a relatively ill-defined copper-silver mixture. DFT pointed towards there being a dynamic surface of copper and silver oxides, which varied strongly as a function of oxygen concentration, but didn't necessarily exist as the surface alloy predicted previously.

To test these theoretical predictions *in situ* XPS was conducted. The catalyst used was an unsupported commercial silver-copper nanopowder purchased from Sigma Aldrich. This was in contrast to the incipient wetness prepared supported catalysts used by Linic *et al.,*[218] and Jankowiak *et al..*[224] Some material differences may have existed between the two systems. The *in situ* XP spectra allowed for assignment of the surface species present as

copper(I)oxide, and copper(II)oxide. Oxidised copper was therefore seen to dominate at the catalyst surface. From XP spectra the atomic ratios of silver, copper, oxygen, and carbon at the surface could then be calculated. Calculating such stoichiometry does have an associated error, as a proportion of the oxygen present could be reacting with the silver. However, the results revealed that there was significantly more copper present, at the catalyst surface, under oxygen rich conditions than in a vacuum. This result was in agreement with the copper-oxygen phases predicted by DFT. Under hydrogen rich conditions the copper content was still enhanced relative to vacuum conditions, although this enhancement was lower, than those seen with oxygen rich or standard reaction conditions. Post-mortem XRD showed diffraction patterns for silver only. The absence of a diffraction pattern for copper is consistent with the hypothesis that only a thin layer of copper might have been present at the catalyst surface. In contrast to the *in situ* results, post reaction TEM showed pure silver surface along with the segregation of copper-oxygen areas. In conclusion the theoretical and experimental results indicated that, during the epoxidation reaction, the catalyst surface may not be comprised of the expected silver-copper species. Instead silver(II)oxide-copper(II)oxide and copper(II)oxide thin films may exist upon the silver substrate. It would be very revealing to explore how reaction conditions impact upon surface coverage for more well-defined catalyst models, such as have been produced in this thesis, under reaction conditions. Raman spectroscopy is also sensitive to both adsorbates and metal-oxygen bonding and so it is envisaged that the TIR Raman technique developed for looking at nanoparticle catalysts could be very valuable in probing the structure-activity relationships really present in this context.

1.6.2. Furfural hydrogenation

The hydrogenation of furfural to furfural alcohol has been the source of much research due to the wide spread use, and chemical importance of the product. Furfural alcohol is an intermediate for a variety of products including plasticizers, lubricants, resins, and dispersing agents.[228–230] Although current industrial catalysts for furfural hydrogenation show reasonable activity and selectivity, the copper chromite catalyst used poses a significant threat to human health.[231,232] Consequently work has been undertaken to find a suitable replacement. A variety of metals (such as nickel, ruthenium, platinum, cobalt, copper) have been investigated as potential catalysts, with reactions trialled in both the vapour and liquid phase.[230,233–236] Platinum catalysts in particular have emerged as a promising candidate for vapour phase furfural hydrogenation,[237–239] and a variety of factors including the support nature and particle size have been shown to be important.[230,237,240,241] Kyriakou *et al.*

atomically dispersed a surface of a catalytically active metal (such as platinum or palladium) onto a more inert support material, which was completely inactive for hydrogenation, in this case copper.[242–245] The group were the first to find that the addition of isolated palladium atoms to a copper surface gave differing catalytic properties to that of copper or palladium alone. This strategy was seen to achieve not only the desired cost reductions, but also to provide significant enhancements in reaction selectivity. The idea investigated in this thesis is based upon that put forward by Kyriakou *et al.* in which the hydrogenation of styrene and acetylene was studied.[245] In collaboration with Aston University (and as is discussed in Chapter 6, Section 6.2, with further introduction to the topic in Section 6.2.1) the doping of atomic quantities of metals such as palladium or platinum onto the surface of copper catalyst (referred to as SAAs) has been undertaken using galvanic displacement. Catalytic testing for furfural hydrogenation has shown enhancements in catalyst selectivity.

1.6.3. Platinum catalysis and nanoparticles

Platinum is a material that is intensively studied in catalysis for its high catalytic activity in many reactions. Key areas in which platinum catalysts are of interest include in the petrochemical and automotive industries. The metal is both corrosion resistant and stable to oxidation at high temperatures.[246] Platinum is often used as a catalyst in organic reactions such as carbon-carbon multiple bond formation, oxidation, hydration, hydrogenation and dehydrogenation.[247] There are many examples of the interesting properties of platinum as well as its creative use, in ways which enhance catalytic properties. For example Chen *et al*. used mesoporous supports,[248] such as SBA-15, to restrict the growth of platinum into nanowires. Using such mesoporous hosts stabilised growth, and prevented agglomeration, such properties are crucial in preparing a reproducible and surface active catalyst. For these reasons, platinum was a metal of interest to study within this thesis. One area of particular interest was that of platinum nanoparticles. Platinum/PVP nps are a system studied within this report, and are focussed upon due their application in ethylene epoxidation (as discussed above in Section 1.6.1.). A schematic of the structure of a platinum/PVP np is illustrated in Figure 1.17 (although not depicted in the figure binding takes place *via* the electronegative oxygen group).

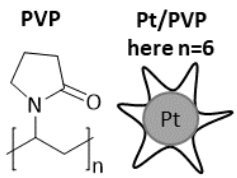

Figure 1.17. Schematic to illustrate the structure of platinum/PVP nps.

1.6.4. Silver catalysts and nanoparticles

Silver finds widespread use in catalysis which is in-part attributed to the high oxidation power of silver-complexes.[249] Use in a variety of areas are seen with examples including: heterogeneous catalysed systems such as NO_x reduction,[250–252] and carbon monoxide oxidation,[253,254] as well as homogeneous examples such as Aldol-type reactions,[255–257] and Michael additions.[258,259] Within this work we focus upon the use of silver nanoparticles with oleylamine and oleic acid capping agents. They are studied by TIR Raman, bimetallic catalysts compromised of silver and copper were also investigated (Chapter 4).

1.6.5. Palladium catalysis and nanoparticles

Palladium finds widespread use in a variety of catalytic transformations: from carbon bond forming reactions such as Heck or Suzuki coupling,[260–265] through to use in heterogeneous catalysis such as in the Lindlar catalyst (which has applications such as selective hydrogenation).[266–268] The doping of sub-stoichometric amounts of palladium, into the traditional copper catalysts used for furfural hydrogenation, has been seen to give unusual and desirable properties (Section 1.6.2). Palladium nanoparticles capped with oleylamine (palladium/OAm nps) where synthesised for use in both TIR Raman studies (see Section 1.4), and the catalytic transformation of cinnamyl alcohol to cinnamaldehyde.[269] In the latter case palladium was chosen as it gave high selectivity of the alcohol to the aldehyde.[270,271] This was important in allowing the challenging cascade reaction of cinnamyl alcohol to cinnamaldehyde and then to cinnamic acid, in which typically side reactions such as cinnanmyl alcohol to 3-phenylpropionaldehyde (in the presence of a platinum catalyst) leads to low product yields (see Chapter 6).[315]

1.7. Aims of the thesis

The work detailed within this thesis aimed firstly to provide new synthetic routes for preparing or modifying nanoparticles as model heterogeneous catalytic systems, and subsequently to develop the use of a surface spectroscopic technique (TIR Raman) for use with such metal nanoparticles, the long term goal being to allow the expansion of the current understanding of mechanisms taking place at catalyst surfaces.

Initial studies using confocal Raman spectroscopy were first undertaken, and allowed for comparison of the TIR Raman technique that was developed, and for clear demonstration of the improved sensitivity of TIR Raman in trying to study species adsorbed on metal nanoparticles. Chapter 3 explores the preparation, deposition (using Langmuir Blodgett techniques), characterisation (using a variety of techniques such as NMR, UV-vis spectroscopy, and mass spectrometry), and study *via* confocal and then TIR Raman of the various nanoparticle systems discussed within Section 1.6. This provided a proof of concept for the use of TIR Raman within the field of *in situ* heterogeneous catalysis studies. Chapter 4 details the development of synthetic routes to prepare copper and copper/silver bimetallics, for intended use in ethylene epoxidation, which is a catalyst system of particular interest to the long term goals of using TIR beyond this study (Section 1.6.1). Chapter 5 then focuses upon the specification, design, construction and setup of a specialist TIR Raman system which was designed and built in house. This system was then used for the study of various nanoparticle systems, synthesised in the previous Chapters. The systematic design of this set-up lead to improvements in reliably sensing sub-monolayer quantities of compounds at the reaction surface. Chapter 6 showcases the applicability of the nanoparticles prepared in this thesis to some additional catalytic reactions of interest by detailing the catalytic testing of nanoparticle systems in applications such as furfural hydrogenation, amide bond formation reactions and selective oxidation. This demonstrated the ability of these nanoparticles to be used for studying and better understanding real catalytic reactions.

1.8. Bibliography

(1) Ertl, G.; Knözinger, H.; Schüth, F.; Weitkamp, J. *Handbook of Heterogeneous Catalysis*, 2nd Edition edition.; Wiley VCH: Weinheim, 2008.

(2) Bond, G. C. *Principles Of Catalysis*; The Royal Institute of Chemistry.

(3) Aris, R.; Bell, A. T.; Boudart, M.; Chen, N. Y.; Gates, B. C.; Haag, W. O.; Somorjai, G. A.; Wei, J.; Hegedus, L. S. *Catalyst Design: Progress and Perspectives*; Wiley-Blackwell: New York, 1987.

(4) Orchin, M. Homogeneous Catalysis: A Wedding of Theory and Experiment. The Eugene J. Houdry Award Address. *Catal. Rev.* **1984**, *26* (1), 59–79.

(5) Richardson, J. T. *Principles of Catalyst Development*; Plenum P: New York, 1989.

(6) Weckhuysen, B. M. Preface: Recent Advances in the in-Situ Characterization of Heterogeneous Catalysts. *Chem. Soc. Rev.* **2010**, *39* (12), 4557–4559.

(7) Bond, G. C. *Catalysis by Metals*; Academic Press Inc, 1962.

(8) Somorjai, G. A.; Beaumont, S. K.; Alayoglu, S. Determination of Molecular Surface Structure, Composition, and Dynamics under Reaction Conditions at High Pressures and at the Solid–Liquid Interface. *Angew. Chem. Int. Ed.* **2011**, *50* (43), 10116–10129.

(9) Somorjai, G. A. *Chemistry in Two Dimensions: Surfaces*; Cornell University Press, 1981.

(10) Beaumont, S. K. Recent Developments in the Application of Nanomaterials to Understanding Molecular Level Processes in Cobalt Catalysed Fischer–Tropsch Synthesis. *Phys. Chem. Chem. Phys.* **2014**, *16* (11), 5034.

(11) Musselwhite, N.; Somorjai, G. A. Investigations of Structure Sensitivity in Heterogeneous Catalysis: From Single Crystals to Monodisperse Nanoparticles. *Top. Catal.* **2013**, *56* (15–17), 1277–1283.

(12) Spencer, N. Iron Single Crystals as Ammonia Synthesis Catalysts: Effect of Surface Structure on Catalyst Activity. *J. Catal.* **1982**, *74* (1), 129–135.

(13) Strongin, D. The Importance of C_7 Sites and Surface Roughness in the Ammonia Synthesis Reaction over Iron. *J. Catal.* **1987**, *103* (1), 213–215.

(14) Asscher, M. The Ammonia Synthesis over Rhenium Single-Crystal Catalysts: Kinetics, Structure Sensitivity, and Effect of Potassium and Oxygen. *J. Catal.* **1986**, *98* (2), 277–287.

(15) Geerlings, J. J. C.; Zonnevylle, M. C.; de Groot, C. P. M. Studies of the Fischer-Tropsch Reaction on Co(0001). *Surf. Sci.* **1991**, *241* (3), 302–314.

(16) Geerlings, I. J. C.; Zonnevylle, M. C.; De Groot, C. P. M. The Fischer-Tropsch Reaction on a Cobalt (0001) Single Crystal. *Catal. Lett.* **1990**, *5* (3), 309–314.

(17) Goodman, D. Kinetics of the Hydrogenation of CO over a Single Crystal Nickel Catalyst. *J. Catal.* **1980**, *63* (1), 226–234.

(18) Goodman, D. W. Single Crystals as Model Catalysts. *J. Vac. Sci. Technol.* **1982**, *20* (3), 522–526.

(19) Goodman, D. W. Model Studies in Catalysis Using Surface Science Probes. *Chem. Rev.* **1995**, *95* (3), 523–536.

(20) Stoltze, P.; Nørskov, J. K. Bridging the "Pressure Gap" between Ultrahigh-Vacuum Surface Physics and High-Pressure Catalysis. *Phys. Rev. Lett.* **1985**, *55* (22), 2502–2505.

(21) Ferrer, S.; Rojo, J. M.; Salmerón, M.; Somorjai, G. A. The Role of Surface Irregularities (Steps, Kinks) and Point Defects on the Chemical Reactivity of Solid Surfaces. *Philos. Mag. A* **1982**, *45* (2), 261–269.

(22) Guthrie, W. L.; Sokol, J. D.; Somorjai, G. A. The Decomposition of Ammonia on the Flat (111) and Stepped (557) Platinum Crystal Surfaces. *Surf. Sci.* **1981**, *109* (2), 390–418.

(23) Gillespie, W. D.; Herz, R. K.; Petersen, E. E.; Somorjai, G. A. The Structure Sensitivity of N-Heptane Dehydrocyclization and Hydrogenolysis Catalyzed by Platinum Single Crystals at Atmospheric Pressure. *J. Catal.* **1981**, *70* (1), 147–159.

(24) Rupprechter, G. Surface Vibrational Spectroscopy from Ultrahigh Vacuum to Atmospheric Pressure: Adsorption and Reactions on Single Crystals and Nanoparticle Model Catalysts Monitored by Sum Frequency Generation Spectroscopy. *Phys. Chem. Chem. Phys.* **2001**, *3* (21), 4621–4632.

(25) Rupprechter, G.; Weilach, C. Spectroscopic Studies of Surface–gas Interactions and Catalyst Restructuring at Ambient Pressure: Mind the Gap! *J. Phys. Condens. Matter* **2008**, *20* (18), 184019.

(26) Dellwig, T.; Rupprechter, G.; Unterhalt, H.; Freund, H.-J. Bridging the Pressure and Materials Gaps: High Pressure Sum Frequency Generation Study on Supported Pd Nanoparticles. *Phys. Rev. Lett.* **2000**, *85* (4), 776–779.

(27) Zaera, F. The Surface Chemistry of Catalysis: New Challenges Ahead. *Surf. Sci.* **2002**, *500* (1–3), 947–965.

(28) Goodman, D. W. Model Catalytic Studies over Metal Single Crystals. *Acc. Chem. Res.* **1984**, *17* (5), 194–200.

(29) Zhang, S.; Nguyen, L.; Zhu, Y.; Zhan, S.; Tsung, C.-K.; Tao, F. In-Situ Studies of Nanocatalysis. *Acc. Chem. Res.* **2013**, *46* (8), 1731–1739.

(30) Grunwaldt, J. D.; Baiker, A. In Situ Spectroscopic Investigation of Heterogeneous Catalysts and Reaction Media at High Pressure. *Phys. Chem. Chem. Phys.* **2005**, *7* (20), 3526.

(31) Clausen, B. S.; Gråbæk, L.; Steffensen, G.; Hansen, P. L.; Topsøe, H. A Combined QEXAFS/XRD Method for on-Line, in Situ Studies of Catalysts: Examples of Dynamic Measurements of Cu-Based Methanol Catalysts. *Catal. Lett.* **1993**, *20* (1–2), 23–36.

(32) Brückner, A. Simultaneous Combination of in Situ-EPR/UV–VIS/On Line GC: A Novel Setup for Investigating Transition Metal Oxide Catalysts under Working Conditions. *Chem. Commun.* **2001**, No. 20, 2122.

(33) McCrea, K. R.; Parker, J. S.; Somorjai, G. A. The Role of Carbon Deposition from CO Dissociation on Platinum Crystal Surfaces during Catalytic CO Oxidation: Effects on Turnover Rate, Ignition Temperature, and Vibrational Spectra. *J. Phys. Chem. B* **2002**, *106* (42), 10854–10863.

(34) Yang, M.; Somorjai, G. A. Adsorption and Reactions of C_6 Hydrocarbons at High Pressures on Pt(111) Single-Crystal Surfaces Studied by Sum Frequency Generation Vibrational Spectroscopy: Mechanisms of Isomerization and Dehydrocyclization of N-Hexane. *J. Am. Chem. Soc.* **2004**, *126* (24), 7698–7708.

(35) Kesmodel, L. L.; Dubois, L. H.; Somorjai, G. A. LEED Analysis of Acetylene and Ethylene Chemisorption on the Pt(111) Surface: Evidence for Ethylidyne Formation. *J. Chem. Phys.* **1979**, *70* (5), 2180–2188.

(36) Demuth, J. E. The Reaction of Ethylene and Acetylene with Pt(111) at Room Temperature: The Formation of Vinyl-like Species. *Surf. Sci.* **1979**, *80*, 367–387.

(37) Salmeron, M.; Somorjai, G. A. Desorption, Decomposition, and Deuterium Exchange Reactions of Unsaturated Hydrocarbons (Ethylene, Acetylene, Propylene, and Butenes) on the platinum(111) Crystal Face. *J. Phys. Chem.* **1982**, *86* (3), 341–350.

(38) Krier, J. M.; Michalak, W. D.; Baker, L. R.; An, K.; Komvopoulos, K.; Somorjai, G. A. Sum Frequency Generation Vibrational Spectroscopy of Colloidal Platinum Nanoparticle Catalysts: Disordering versus Removal of Organic Capping. *J. Phys. Chem. C* **2012**, *116* (33), 17540–17546.

(39) Baker, L. R.; Kennedy, G.; Krier, J.; Spronsen, M.; Onorato, R.; Somorjai, G. The Role of an Organic Cap in Nanoparticle Catalysis: Reversible Restructuring of Carbonaceous Material Controls Catalytic Activity of Platinum Nanoparticles for

Ethylene Hydrogenation and Methanol Oxidation. *Catal. Lett.* **2012**, *142* (11), 1286–1294.

(40) Haw, J. F. *In-situ Spectroscopy in Heterogeneous Catalysis*; Wiley VCH: Weinheim, 2002.

(41) Andanson, J. M.; Baiker, A. Exploring Catalytic Solid/Liquid Interfaces by in Situ Attenuated Total Reflection Infrared Spectroscopy. *Chem. Soc. Rev.* **2010**, *39* (12), 4571–4584.

(42) Weckhuysen, B. M. *In-Situ Spectroscopy of Catalysts: 1*; American Scientific Publishers: Stevenson Ranch, Calif., 2004.

(43) He, C.; Zhang, G.; Ke, J.; Zhang, H.; Miller, J. T.; Kropf, A. J.; Lei, A. Labile Cu(I) Catalyst/Spectator Cu(II) Species in Copper-Catalyzed C–C Coupling Reaction: Operando IR, in Situ XANES/EXAFS Evidence and Kinetic Investigations. *J. Am. Chem. Soc.* **2013**, *135* (1), 488–493.

(44) Bordiga, S.; Groppo, E.; Agostini, G.; van Bokhoven, J. A.; Lamberti, C. Reactivity of Surface Species in Heterogeneous Catalysts Probed by In Situ X-Ray Absorption Techniques. *Chem. Rev.* **2013**, *113* (3), 1736–1850.

(45) Wong, S. T.; Lee, J. F.; Cheng, S.; Mou, C. Y. In-Situ Study of MCM-41-Supported Iron Oxide Catalysts by XANES and EXAFS. *Appl. Catal. Gen.* **2000**, *198* (1–2), 115–126.

(46) Teo, D. B. K. EXAFS Parameters. In *EXAFS: Basic Principles and Data Analysis*; Inorganic Chemistry Concepts; Springer Berlin Heidelberg, 1986; pp 34–52.

(47) Clausen, B. S.; Steffensen, G.; Fabius, B.; Villadsen, J.; Feidenhans'l, R.; Topsøe, H. In Situ Cell for Combined XRD and on-Line Catalysis Tests: Studies of Cu-Based Water Gas Shift and Methanol Catalysts. *J. Catal.* **1991**, *132* (2), 524–535.

(48) Thomas, J. M.; Sankar, G. The Role of XAFS in the *in Situ* and *Ex Situ* Elucidation of Active Sites in Designed Solid Catalysts. *J. Synchrotron Radiat.* **2001**, *8* (2), 55–60.

(49) Grunwaldt, J. D.; Clausen, B. S. Combining XRD and EXAFS with on-Line Catalytic Studies for in Situ Characterization of Catalysts. *Top. Catal.* **2002**, *18* (1–2), 37–43.

(50) Grunwaldt, J. D.; Caravati, M.; Hannemann, S.; Baiker, A. X-Ray Absorption Spectroscopy under Reaction Conditions: Suitability of Different Reaction Cells for Combined Catalyst Characterization and Time-Resolved Studies. *Phys. Chem. Chem. Phys.* **2004**, *6* (11), 3037–3047.

(51) Hannemann, S.; Casapu, M.; Grunwaldt, J. D.; Haider, P.; Trüssel, P.; Baiker, A.; Welter, E. A Versatile in Situ Spectroscopic Cell for Fluorescence/Transmission EXAFS

and X-Ray Diffraction of Heterogeneous Catalysts in Gas and Liquid Phase. *J. Synchrotron Radiat.* **2007**, *14* (4), 345–354.

(52) Hannemann, S.; Grunwaldt, J.-D.; Lienemann, P.; Günther, D.; Krumeich, F.; Pratsinis, S. E.; Baiker, A. Combination of Flame Synthesis and High-Throughput Experimentation: The Preparation of Alumina-Supported Noble Metal Particles and Their Application in the Partial Oxidation of Methane. *Appl. Catal. Gen.* **2007**, *316* (2), 226–239.

(53) Stark, W. J.; Grunwaldt, J. D.; Maciejewski, M.; Pratsinis, S. E.; Baiker, A. Flame-Made Pt/Ceria/Zirconia for Low-Temperature Oxygen Exchange. *Chem. Mater.* **2005**, *17* (13), 3352–3358.

(54) Ruban, A. V.; Skriver, H. L.; Nørskov, J. K. Surface Segregation Energies in Transition-Metal Alloys. *Phys. Rev. B* **1999**, *59* (24), 15990–16000.

(55) Casapu, M.; Grunwaldt, J. D.; Maciejewski, M.; Wittrock, M.; Göbel, U.; Baiker, A. Formation and Stability of Barium Aluminate and Cerate in NO_x Storage-Reduction Catalysts. *Appl. Catal. B Environ.* **2006**, *63* (3–4), 232–242.

(56) Burda, C.; Chen, X.; Narayanan, R.; El-Sayed, M. A. Chemistry and Properties of Nanocrystals of Different Shapes. *Chem. Rev.* **2005**, *105* (4), 1025–1102.

(57) Somorjai, G. A. Modern Concepts in Surface Science and Heterogeneous Catalysis. *J. Phys. Chem.* **1990**, *94* (3), 1013–1023.

(58) Jacobs, G.; Chaney, J. A.; Patterson, P. M.; Das, T. K.; Davis, B. H. Fischer–Tropsch Synthesis: Study of the Promotion of Re on the Reduction Property of Co/Al_2O_3 Catalysts by in Situ EXAFS/XANES of Co K and Re LIII Edges and XPS. *Appl. Catal. Gen.* **2004**, *264* (2), 203–212.

(59) Skoplyak, O.; Barteau, M. A.; Chen, J. G. Ethanol and Ethylene Glycol on Ni/Pt(111) Bimetallic Surfaces: A DFT and HREELS Study. *Surf. Sci.* **2008**, *602* (23), 3578–3587.

(60) Tao, F.; Dag, S.; Wang, L.-W.; Liu, Z.; Butcher, D. R.; Bluhm, H.; Salmeron, M.; Somorjai, G. A. Break-Up of Stepped Platinum Catalyst Surfaces by High CO Coverage. *Science* **2010**, *327* (5967), 850–853.

(61) Pearl, T. P.; Sibener, S. J. Oxygen Driven Reconstruction Dynamics of Ni(977) Measured by Time-Lapse Scanning Tunneling Microscopy. *J. Chem. Phys.* **2001**, *115* (4), 1916–1927.

(62) Wachs, I. E.; Roberts, C. A. Monitoring Surface Metal Oxide Catalytic Active Sites with Raman Spectroscopy. *Chem. Soc. Rev.* **2010**, *39* (12), 5002–5017.

(63) Tyrode, E.; Rutland, M. W.; Bain, C. D. Adsorption of CTAB on Hydrophilic Silica Studied by Linear and Nonlinear Optical Spectroscopy. *J. Am. Chem. Soc.* **2008**, *130* (51), 17434–17445.

(64) Mestl, G. In Situ Raman Spectroscopy — a Valuable Tool to Understand Operating Catalysts. *J. Mol. Catal. Chem.* **2000**, *158* (1), 45–65.

(65) Knözinger, H.; Mestl, G. Laser Raman Spectroscopy–a Powerful Tool for in Situ Studies of Catalytic Materials. *Top. Catal.* **1999**, *8* (1–2), 45–55.

(66) Carette, J. D.; Feuerbacher, B.; Ibach, H. *Electron Spectroscopy for Surface Analysis*, Softcover reprint of the original 1st ed. 1977 edition.; Springer: Berlin, Heidelberg, 2012.

(67) Jaffé, H. H. *Theory and Applications of Ultraviolet Spectroscopy*; Wiley: New York, 1962.

(68) Bañares, M. A.; Wachs, I. E. Molecular Structures of Supported Metal Oxide Catalysts under Different Environments. *J. Raman Spectrosc.* **2002**, *33* (5), 359–380.

(69) Cheng, S.; Yang, L.; Chen, D.; Ji, X.; Jiang, Z.; Ding, D.; Liu, M. Phase Evolution of an Alpha MnO_2-Based Electrode for Pseudo-Capacitors Probed by in Operando Raman Spectroscopy. *Nano Energy* **2014**, *9*, 161–167.

(70) Whitney, A. V.; Elam, J. W.; Stair, P. C.; Van Duyne, R. P. Toward a Thermally Robust Operando Surface-Enhanced Raman Spectroscopy Substrate. *J. Phys. Chem. C* **2007**, *111* (45), 16827–16832.

(71) Xu, J.; Deng, Y. Q.; Luo, Y.; Mao, W.; Yang, X. J.; Han, Y.-F. Operando Raman Spectroscopy and Kinetic Study of Low-Temperature CO Oxidation on an α-Mn_2O_3 Nanocatalyst. *J. Catal.* **2013**, *300*, 225–234.

(72) Bañares, M. A.; Guerrero-Pérez, M. O.; Fierro, J. L. G.; Cortez, G. G. Raman Spectroscopy during Catalytic Operations with on-Line Activity Measurement (Operando Spectroscopy): A Method for Understanding the Active Centres of Cations Supported on Porous Materials. *J Mater Chem* **2002**, *12* (11), 3337–3342.

(73) Brandhorst, M.; Cristol, S.; Capron, M.; Dujardin, C.; Vezin, H.; Le bourdon, G.; Payen, E. Catalytic Oxidation of Methanol on Mo/Al_2O_3 Catalyst: An EPR and Raman/Infrared Operando Spectroscopies Study. *Catal. Today* **2006**, *113* (1–2), 34–39.

(74) Guerrero-Pérez, M. O.; Herrera, M. C.; Malpartida, I.; Larrubia, M. A.; Alemany, L. J.; Bañares, M. A. Operando Raman Study of Propane Oxidation over Alumina-Supported V–Mo–W–O Catalysts. *Catal. Today* **2007**, *126* (1–2), 177–183.

(75) Tinnemans, S. J.; Kox, M. H. F.; Nijhuis, T. A.; Visser, T.; Weckhuysen, B. M. Real Time Quantitative Raman Spectroscopy of Supported Metal Oxide Catalysts without the Need of an Internal Standard. *Phys. Chem. Chem. Phys.* **2005**, *7* (1), 211–216.

(76) O'Grady, A.; Dennis, A. C.; Denvir, D.; McGarvey, J. J.; Bell, S. E. J. Quantitative Raman Spectroscopy of Highly Fluorescent Samples Using Pseudosecond Derivatives and Multivariate Analysis. *Anal. Chem.* **2001**, *73* (9), 2058–2065.

(77) Picard, A.; Daniel, I.; Montagnac, G.; Oger, P. In Situ Monitoring by Quantitative Raman Spectroscopy of Alcoholic Fermentation by Saccharomyces Cerevisiae under High Pressure. *Extremophiles* **2007**, *11* (3), 445–452.

(78) Woods, D. A.; Bain, C. D. Total Internal Reflection Raman Spectroscopy. *Analyst* **2012**, *137* (1), 35–48.

(79) Michaels, C. A. Surface-Sensitive Raman Microscopy with Total Internal Reflection Illumination. *J. Raman Spectrosc.* **2010**, *41* (12), 1670–1677.

(80) Bain, G. Total Internal Reflection Raman Spectroscopy. Spectroscopy Europe 2004.

(81) Knorr, F.; Smith, Z. J.; Wachsmann-Hogiu, S. Development of a Time-Gated System for Raman Spectroscopy of Biological Samples. *Opt. Express* **2010**, *18* (19), 20049.

(82) Kostamovaara, J.; Tenhunen, J.; Kögler, M.; Nissinen, I.; Nissinen, J.; Keränen, P. Fluorescence Suppression in Raman Spectroscopy Using a Time-Gated CMOS SPAD. *Opt. Express* **2013**, *21* (25), 31632.

(83) Mahajan, S.; Cole, R. M.; Speed, J. D.; Pelfrey, S. H.; Russell, A. E.; Bartlett, P. N.; Barnett, S. M.; Baumberg, J. J. Understanding the Surface-Enhanced Raman Spectroscopy "Background" †. *J. Phys. Chem. C* **2010**, *114* (16), 7242–7250.

(84) Stiles, P. L.; Dieringer, J. A.; Shah, N. C.; Van Duyne, R. P. Surface-Enhanced Raman Spectroscopy. *Annu. Rev. Anal. Chem.* **2008**, *1* (1), 601–626.

(85) Brown, K. R.; Walter, D. G.; Natan, M. J. Seeding of Colloidal Au Nanoparticle Solutions. 2. Improved Control of Particle Size and Shape. *Chem. Mater.* **2000**, *12* (2), 306–313.

(86) Yang, Y.; Gong, X.; Zeng, H.; Zhang, L.; Zhang, X.; Zou, C.; Huang, S. Combination of Digestive Ripening and Seeding Growth As a Generalized Route for Precisely Controlling Size of Monodispersed Noble Monometallic, Shell Thickness of Core-Shell and Composition of Alloy Nanoparticles. *J. Phys. Chem. C* **2009**, *114* (1), 256–264.

(87) Buck, M. R.; Biacchi, A. J.; Schaak, R. E. Insights into the Thermal Decomposition of Co(II) Oleate for the Shape-Controlled Synthesis of Wurtzite-Type CoO Nanocrystals. *Chem. Mater.* **2014**, *26* (3), 1492–1499.

(88) Zhang, Q.; Xie, J.; Yang, J.; Lee, J. Y. Monodisperse Icosahedral Ag, Au, and Pd Nanoparticles: Size Control Strategy and Superlattice Formation. *ACS Nano* **2009**, *3* (1), 139–148.

(89) Maye, M. M.; Zheng, W.; Leibowitz, F. L.; Ly, N. K.; Zhong, C.-J. Heating-Induced Evolution of Thiolate-Encapsulated Gold Nanoparticles: A Strategy for Size and Shape Manipulations. *Langmuir* **1999**, *16* (2), 490–497.

(90) Chaudret, B. Synthesis and Surface Reactivity of Organometallic Nanoparticles. In *Surface and Interfacial Organometallic Chemistry and Catalysis*; Copéret, C., Chaudret, B., Eds.; Springer Berlin Heidelberg, 2005; Vol. 16, pp 233–259.

(91) Andersson, M. P.; Abild-Pedersen, F.; Remediakis, I. N.; Bligaard, T.; Jones, G.; Engbæk, J.; Lytken, O.; Horch, S.; Nielsen, J. H.; Sehested, J.; Rostrup-Nielsen, J. R.; Nørskov, J. K.; Chorkendorff, I. Structure Sensitivity of the Methanation Reaction: H_2-Induced CO Dissociation on Nickel Surfaces. *J. Catal.* **2008**, *255* (1), 6–19.

(92) Kliewer, C. J.; Bieri, M.; Somorjai, G. A. Hydrogenation of the A,β-Unsaturated Aldehydes Acrolein, Crotonaldehyde, and Prenal over Pt Single Crystals: A Kinetic and Sum-Frequency Generation Vibrational Spectroscopy Study. *J. Am. Chem. Soc.* **2009**, *131* (29), 9958–9966.

(93) Bratlie, K. M.; Lee, H.; Komvopoulos, K.; Yang, P.; Somorjai, G. A. Platinum Nanoparticle Shape Effects on Benzene Hydrogenation Selectivity. *Nano Lett.* **2007**, *7* (10), 3097–3101.

(94) Kuhn, J. N.; Huang, W.; Tsung, C.-K.; Zhang, Y.; Somorjai, G. A. Structure Sensitivity of Carbon−Nitrogen Ring Opening: Impact of Platinum Particle Size from below 1 to 5 Nm upon Pyrrole Hydrogenation Product Selectivity over Monodisperse Platinum Nanoparticles Loaded onto Mesoporous Silica. *J. Am. Chem. Soc.* **2008**, *130* (43), 14026–14027.

(95) Somorjai, G. A.; Frei, H.; Park, J. Y. Advancing the Frontiers in Nanocatalysis, Biointerfaces, and Renewable Energy Conversion by Innovations of Surface Techniques. *J. Am. Chem. Soc.* **2009**, *131* (46), 16589–16605.

(96) Zhu, J.; Somorjai, G. A. Formation of Platinum Silicide on a Platinum Nanoparticle Array Model Catalyst Deposited on Silica during Chemical Reaction. *Nano Lett.* **2001**, *1* (1), 8–13.

(97) Rioux, R. M.; Song, H.; Hoefelmeyer, J. D.; Yang, P.; Somorjai, G. A. High-Surface-Area Catalyst Design: Synthesis, Characterization, and Reaction Studies of Platinum Nanoparticles in Mesoporous SBA-15 Silica †. *J. Phys. Chem. B* **2005**, *109* (6), 2192–2202.

(98) Zhao, C. X.; He, L.; Qiao, S. Z.; Middelberg, A. P. J. Nanoparticle Synthesis in Microreactors. *Chem. Eng. Sci.* **2011**, *66* (7), 1463–1479.

(99) Chan, H. K.; Kwok, P. C. L. Production Methods for Nanodrug Particles Using the Bottom-up Approach. *Adv. Drug Deliv. Rev.* **2011**, *63* (6), 406–416.

(100) Lam, C.; Zhang, Y. .; Tang, Y. .; Lee, C. .; Bello, I.; Lee, S. . Large-Scale Synthesis of Ultrafine Si Nanoparticles by Ball Milling. *J. Cryst. Growth* **2000**, *220* (4), 466–470.

(101) Wang, Y.; Xia, Y. Bottom-Up and Top-Down Approaches to the Synthesis of Monodispersed Spherical Colloids of Low Melting-Point Metals. *Nano Lett.* **2004**, *4* (10), 2047–2050.

(102) Ayyappan, S.; Gopalan, R. S.; Subbanna, G. N.; Rao, C. N. R. Nanoparticles of Ag, Au, Pd, and Cu Produced by Alcohol Reduction of the Salts. *J. Mater. Res.* **1997**, *12* (02), 398–401.

(103) Sun, S. Monodisperse FePt Nanoparticles and Ferromagnetic FePt Nanocrystal Superlattices. *Science* **2000**, *287* (5460), 1989–1992.

(104) Sakai, T.; Alexandridis, P. Mechanism of Gold Metal Ion Reduction, Nanoparticle Growth and Size Control in Aqueous Amphiphilic Block Copolymer Solutions at Ambient Conditions. *J. Phys. Chem. B* **2005**, *109* (16), 7766–7777.

(105) Jana, N. R.; Gearheart, L.; Murphy, C. J. Evidence for Seed-Mediated Nucleation in the Chemical Reduction of Gold Salts to Gold Nanoparticles. *Chem. Mater.* **2001**, *13* (7), 2313–2322.

(106) Mohamed Mathar Sahib, I. K.; Thangaraju, D.; Prakash, N.; Masuda, Y.; Inami, W.; Kawata, Y.; Hayakawa, Y. Size Controlled Synthesis of Silver Sulfide Nanostructures by Multi-Solvent Thermal Decomposition Method. *J. Cryst. Growth* **2016**.

(107) Navaladian, S.; Viswanathan, B.; Viswanath, R. P.; Varadarajan, T. K. Thermal Decomposition as Route for Silver Nanoparticles. *Nanoscale Res. Lett.* **2007**, *2* (1), 44–48.

(108) Salavati-Niasari, M.; Davar, F. Synthesis of Copper and Copper (I) Oxide Nanoparticles by Thermal Decomposition of a New Precursor. *Mater. Lett.* **2009**, *63* (3), 441–443.

(109) Maity, D.; Kale, S. N.; Kaul-Ghanekar, R.; Xue, J. M.; Ding, J. Studies of Magnetite Nanoparticles Synthesized by Thermal Decomposition of Iron (III) Acetylacetonate in Tri(ethylene Glycol). *J. Magn. Magn. Mater.* **2009**, *321* (19), 3093–3098.

(110) Yang, Y.; Chen, H.; Zhao, B.; Bao, X. Size Control of ZnO Nanoparticles via Thermal Decomposition of Zinc Acetate Coated on Organic Additives. *J. Cryst. Growth* **2004**, *263* (1), 447–453.

(111) Salavati-Niasari, M.; Davar, F.; Mazaheri, M.; Shaterian, M. Preparation of Cobalt Nanoparticles from [bis(salicylidene)cobalt(II)]–oleylamine Complex by Thermal Decomposition. *J. Magn. Magn. Mater.* **2008**, *320* (3–4), 575–578.

(112) Cumberland, S. A.; Lead, J. R. Particle Size Distributions of Silver Nanoparticles at Environmentally Relevant Conditions. *J. Chromatogr. A* **2009**, *1216* (52), 9099–9105.

(113) Prathna, T. C.; Chandrasekaran, N.; Mukherjee, A. Studies on Aggregation Behaviour of Silver Nanoparticles in Aqueous Matrices: Effect of Surface Functionalization and Matrix Composition. *Colloids Surf. Physicochem. Eng. Asp.* **2011**, *390* (1–3), 216–224.

(114) Christian, P.; Von der Kammer, F.; Baalousha, M.; Hofmann, T. Nanoparticles: Structure, Properties, Preparation and Behaviour in Environmental Media. *Ecotoxicology* **2008**, *17* (5), 326–343.

(115) Lopez-Sanchez, J. A.; Dimitratos, N.; Hammond, C.; Brett, G. L.; Kesavan, L.; White, S.; Miedziak, P.; Tiruvalam, R.; Jenkins, R. L.; Carley, A. F.; Knight, D.; Kiely, C. J.; Hutchings, G. J. Facile Removal of Stabilizer-Ligands from Supported Gold Nanoparticles. *Nat. Chem.* **2011**, *3* (7), 551–556.

(116) He, F.; Zhao, D. Manipulating the Size and Dispersibility of Zerovalent Iron Nanoparticles by Use of Carboxymethyl Cellulose Stabilizers. *Environ. Sci. Technol.* **2007**, *41* (17), 6216–6221.

(117) Chen, J.; Wang, J.; Zhang, X.; Jin, Y. Microwave-Assisted Green Synthesis of Silver Nanoparticles by Carboxymethyl Cellulose Sodium and Silver Nitrate. *Mater. Chem. Phys.* **2008**, *108* (2–3), 421–424.

(118) Huang, H.; Yang, X. Synthesis of Polysaccharide-Stabilized Gold and Silver Nanoparticles: A Green Method. *Carbohydr. Res.* **2004**, *339* (15), 2627–2631.

(119) Park, Y.; Hong, Y. N.; Weyers, A.; Kim, Y. S.; Linhardt, R. J. Polysaccharides and Phytochemicals: A Natural Reservoir for the Green Synthesis of Gold and Silver Nanoparticles. *IET Nanobiotechnol.* **2011**, *5* (3), 69.

(120) Zhang, H.; Wang, R.; Zhang, G.; Yang, B. A Covalently Attached Film Based on Poly(methacrylic Acid)-Capped Fe_3O_4 Nanoparticles. *Thin Solid Films* **2003**, *429* (1–2), 167–173.

(121) Stevanović, M.; Bračko, I.; Milenković, M.; Filipović, N.; Nunić, J.; Filipič, M.; Uskoković, D. P. Multifunctional PLGA Particles Containing Poly(l-Glutamic Acid)-Capped Silver Nanoparticles and Ascorbic Acid with Simultaneous Antioxidative and Prolonged Antimicrobial Activity. *Acta Biomater.* **2014**, *10* (1), 151–162.

(122) Narayanan, R.; El-Sayed, M. A. Effect of Colloidal Catalysis on the Nanoparticle Size Distribution: Dendrimer−Pd vs PVP−Pd Nanoparticles Catalyzing the Suzuki Coupling Reaction †. *J. Phys. Chem. B* **2004**, *108* (25), 8572–8580.

(123) Lévy, R.; Thanh, N. T. K.; Doty, R. C.; Hussain, I.; Nichols, R. J.; Schiffrin, D. J.; Brust, M.; Fernig, D. G. Rational and Combinatorial Design of Peptide Capping Ligands for Gold Nanoparticles. *J. Am. Chem. Soc.* **2004**, *126* (32), 10076–10084.

(124) Kim, S.-W.; Park, J.; Jang, Y.; Chung, Y.; Hwang, S.; Hyeon, T.; Kim, Y. W. Synthesis of Monodisperse Palladium Nanoparticles. *Nano Lett.* **2003**, *3* (9), 1289–1291.

(125) Taleb, A.; Petit, C.; Pileni, M. P. Synthesis of Highly Monodisperse Silver Nanoparticles from AOT Reverse Micelles: A Way to 2D and 3D Self-Organization. *Chem. Mater.* **1997**, *9* (4), 950–959.

(126) Boutonnet, M. Monodisperse Colloidal Metal Particles from Nonaqueous Solutions: Catalytic Behavior in Hydrogenation of but-1-Ene of Platinum, Palladium, and Rhodium Particles Supported on Pumice. *J. Catal.* **1987**, *103* (1), 95–104.

(127) Calò, V.; Nacci, A.; Monopoli, A.; Montingelli, F. Pd Nanoparticles as Efficient Catalysts for Suzuki and Stille Coupling Reactions of Aryl Halides in Ionic Liquids. *J. Org. Chem.* **2005**, *70* (15), 6040–6044.

(128) Venkatesan, R.; Prechtl, M. H. G.; Scholten, J. D.; Pezzi, R. P.; Machado, G.; Dupont, J. Palladium Nanoparticle Catalysts in Ionic Liquids: Synthesis, Characterisation and Selective Partial Hydrogenation of Alkynes to Z-Alkenes. *J. Mater. Chem.* **2011**, *21* (9), 3030.

(129) Kuhn, J. N.; Tsung, C. K.; Huang, W.; Somorjai, G. A. Effect of Organic Capping Layers over Monodisperse Platinum Nanoparticles upon Activity for Ethylene Hydrogenation and Carbon Monoxide Oxidation. *J. Catal.* **2009**, *265* (2), 209–215.

(130) Aliaga, C.; Park, J. Y.; Yamada, Y.; Lee, H. S.; Tsung, C. K.; Yang, P.; Somorjai, G. A. Sum Frequency Generation and Catalytic Reaction Studies of the Removal of Organic

Capping Agents from Pt Nanoparticles by UV−Ozone Treatment. *J. Phys. Chem. C* **2009**, *113* (15), 6150–6155.

(131) Kim, J. H.; Park, J. S.; Chung, H. W.; Boote, B. W.; Lee, T. R. Palladium Nanoshells Coated with Self-Assembled Monolayers and Their Catalytic Properties. *RSC Adv.* **2012**, *2* (9), 3968.

(132) Makosch, M.; Lin, W.-I.; Bumbálek, V.; Sá, J.; Medlin, J. W.; Hungerbühler, K.; van Bokhoven, J. A. Organic Thiol Modified Pt/TiO_2 Catalysts to Control Chemoselective Hydrogenation of Substituted Nitroarenes. *ACS Catal.* **2012**, *2* (10), 2079–2081.

(133) Yan, M.; Jin, T.; Ishikawa, Y.; Minato, T.; Fujita, T.; Chen, L. Y.; Bao, M.; Asao, N.; Chen, M.-W.; Yamamoto, Y. Nanoporous Gold Catalyst for Highly Selective Semihydrogenation of Alkynes: Remarkable Effect of Amine Additives. *J. Am. Chem. Soc.* **2012**, *134* (42), 17536–17542.

(134) Mitsudome, T.; Takahashi, Y.; Ichikawa, S.; Mizugaki, T.; Jitsukawa, K.; Kaneda, K. Metal-Ligand Core-Shell Nanocomposite Catalysts for the Selective Semihydrogenation of Alkynes. *Angew. Chem. Int. Ed.* **2013**, *52* (5), 1481–1485.

(135) Ghosh, A.; Basak, S.; Wunsch, B. H.; Kumar, R.; Stellacci, F. Effect of Composition on the Catalytic Properties of Mixed-Ligand-Coated Gold Nanoparticles. *Angew. Chem. Int. Ed.* **2011**, *50* (34), 7900–7905.

(136) Baker, L. R.; Kennedy, G.; Krier, J.; Spronsen, M.; Onorato, R.; Somorjai, G. The Role of an Organic Cap in Nanoparticle Catalysis: Reversible Restructuring of Carbonaceous Material Controls Catalytic Activity of Platinum Nanoparticles for Ethylene Hydrogenation and Methanol Oxidation. *Catal. Lett.* **2012**, *142* (11), 1286–1294.

(137) Roy, P. S.; Bhattacharya, S. K. Size-Controlled Synthesis and Characterization of Polyvinyl Alcohol-Coated Platinum Nanoparticles: Role of Particle Size and Capping Polymer on the Electrocatalytic Activity. *Catal. Sci. Technol.* **2013**, *3* (5), 1314–1323.

(138) LaMer, V. K.; Dinegar, R. H. Theory, Production and Mechanism of Formation of Monodispersed Hydrosols. *J. Am. Chem. Soc.* **1950**, *72* (11), 4847–4854.

(139) Mer, V. K. L. Nucleation in Phase Transitions. *Ind. Eng. Chem.* **1952**, *44* (6), 1270–1277.

(140) Cushing, B. L.; Kolesnichenko, V. L.; O'Connor, C. J. Recent Advances in the Liquid-Phase Syntheses of Inorganic Nanoparticles. *Chem. Rev.* **2004**, *104* (9), 3893–3946.

(141) Anderson, V. J.; Lekkerkerker, H. N. W. Insights into Phase Transition Kinetics from Colloid Science. *Nature* **2002**, *416* (6883), 811–815.

(142) Ostwald, W. Studien Über Die Bildung Und Umwandlung Fester Körper. *Z Phys Chem* **1897**, *22*, 289–330.

(143) Ostwald, W. *Lehrbuch Der Allgemeinen Chemie, Vol. 2, Part 1. Engelmann, Leipzig, Germany*; German, 1896.

(144) Ostwald, W. On the Assumed Isomerism of Red and Yellow Mercury Oxide and the Surface-Tension of Solid Bodies. *Z Phys Chem* **1900**, *34*, 495.

(145) Lin, X. M.; Sorensen, C. M.; Klabunde, K. J. Digestive Ripening, Nanophase Segregation and Superlattice Formation in Gold Nanocrystal Colloids. *J. Nanoparticle Res.* **2000**, *2* (2), 157–164.

(146) Sahu, P.; Prasad, B. L. V. Time and Temperature Effects on the Digestive Ripening of Gold Nanoparticles: Is There a Crossover from Digestive Ripening to Ostwald Ripening? *Langmuir* **2014**, *30* (34), 10143–10150.

(147) Lin, X. M.; Wang, G. M.; Sorensen, C. M.; Klabunde, K. J. Formation and Dissolution of Gold Nanocrystal Superlattices in a Colloidal Solution. *J. Phys. Chem. B* **1999**, *103* (26), 5488–5492.

(148) *Nanostructured and Advanced Materials for Applications in Sensor, Optoelectronic and Photovoltaic Technology*; Vaseashta, A., Dimova-Malinovska, D., Marshall, J. M., Eds.; NATO Science Series II: Mathematics, Physics and Chemistry; Springer Netherlands: Dordrecht, 2005; Vol. 204.

(149) Prasad, B. L. V.; Stoeva, S. I.; Sorensen, C. M.; Klabunde, K. J. Digestive-Ripening Agents for Gold Nanoparticles: Alternatives to Thiols. *Chem. Mater.* **2003**, *15* (4), 935–942.

(150) Pan, C.; Pelzer, K.; Philippot, K.; Chaudret, B.; Dassenoy, F.; Lecante, P.; Casanove, M.-J. Ligand-Stabilized Ruthenium Nanoparticles: Synthesis, Organization, and Dynamics. *J. Am. Chem. Soc.* **2001**, *123* (31), 7584–7593.

(151) Zheng, N.; Fan, J.; Stucky, G. D. One-Step One-Phase Synthesis of Monodisperse Noble-Metallic Nanoparticles and Their Colloidal Crystals. *J. Am. Chem. Soc.* **2006**, *128* (20), 6550–6551.

(152) Jana, N. R.; Peng, X. Single-Phase and Gram-Scale Routes toward Nearly Monodisperse Au and Other Noble Metal Nanocrystals. *J. Am. Chem. Soc.* **2003**, *125* (47), 14280–14281.

(153) Samia, A. C. S.; Schlueter, J. A.; Jiang, J. S.; Bader, S. D.; Qin, C.-J.; Lin, X.-M. Effect of Ligand−Metal Interactions on the Growth of Transition-Metal and Alloy Nanoparticles. *Chem. Mater.* **2006**, *18* (22), 5203–5212.

(154) Zhang, Q.; Xie, J.; Yu, Y.; Lee, J. Y. Monodispersity Control in the Synthesis of Monometallic and Bimetallic Quasi-Spherical Gold and Silver Nanoparticles. *Nanoscale* **2010**, *2* (10), 1962.

(155) Hiramatsu, H.; Osterloh, F. E. A Simple Large-Scale Synthesis of Nearly Monodisperse Gold and Silver Nanoparticles with Adjustable Sizes and with Exchangeable Surfactants. *Chem. Mater.* **2004**, *16* (13), 2509–2511.

(156) Porel, S.; Singh, S.; Harsha, S. S.; Rao, D. N.; Radhakrishnan, T. P. Nanoparticle-Embedded Polymer: In Situ Synthesis, Free-Standing Films with Highly Monodisperse Silver Nanoparticles and Optical Limiting. *Chem. Mater.* **2005**, *17* (1), 9–12.

(157) Teranishi, T.; Hosoe, M.; Tanaka, T.; Miyake, M. Size Control of Monodispersed Pt Nanoparticles and Their 2D Organization by Electrophoretic Deposition. *J. Phys. Chem. B* **1999**, *103* (19), 3818–3827.

(158) Tlili, A.; Monnier, F.; Taillefer, M. Selective One-Pot Synthesis of Symmetrical and Unsymmetrical Di- and Triarylamines with a Ligandless Copper Catalytic System. *Chem. Commun.* **2012**, *48* (51), 6408.

(159) Yefremenko, I. G.; Zilberberg, I. L.; Zhidomirov, G. M.; Pak, A. M. Hydrogen Activation on Copper Catalytic Sites in Stereoselective Alkyne Hydrogenation. *React. Kinet. Catal. Lett.* **1995**, *56* (1), 77–86.

(160) Jia, Z.; Bell, C. A.; Monteiro, M. J. Directing the Pathway of Orthogonal “click” Reactions by Modulating Copper-Catalytic Activity. *Chem. Commun.* **2011**, *47* (14), 4165.

(161) Barbero, N.; SanMartin, R.; Domínguez, E. An Efficient Copper-Catalytic System for Performing Intramolecular O-Arylation Reactions in Aqueous Media. New Synthesis of Xanthones. *Green Chem.* **2009**, *11* (6), 830.

(162) Lee, Y.; Choi, J.; Lee, K. J.; Stott, N. E.; Kim, D. Large-Scale Synthesis of Copper Nanoparticles by Chemically Controlled Reduction for Applications of Inkjet-Printed Electronics. *Nanotechnology* **2008**, *19* (41), 415604.

(163) Hwang, H. J.; Chung, W. H.; Kim, H. S. *In Situ* Monitoring of Flash-Light Sintering of Copper Nanoparticle Ink for Printed Electronics. *Nanotechnology* **2012**, *23* (48), 485205.

(164) Kang, B.; Han, S.; Kim, J.; Ko, S.; Yang, M. One-Step Fabrication of Copper Electrode by Laser-Induced Direct Local Reduction and Agglomeration of Copper Oxide Nanoparticle. *J. Phys. Chem. C* **2011**, *115* (48), 23664–23670.

(165) *CRC Handbook of Chemistry and Physics, 95th Edition*, 95 edition.; Haynes, W. M., Ed.; CRC Press: Boca Raton; London; New York, 2014.

(166) Li, J. Y.; Xiong, S.; Pan, J.; Qian, Y. Hydrothermal Synthesis and Electrochemical Properties of Urchin-Like Core−Shell Copper Oxide Nanostructures. *J. Phys. Chem. C* **2010**, *114* (21), 9645–9650.

(167) Grouchko, M.; Kamyshny, A.; Magdassi, S. Formation of Air-Stable Copper–silver Core–shell Nanoparticles for Inkjet Printing. *J. Mater. Chem.* **2009**, *19* (19), 3057–3062.

(168) Saison, C.; Perreault, F.; Daigle, J. C.; Fortin, C.; Claverie, J.; Morin, M.; Popovic, R. Effect of Core–shell Copper Oxide Nanoparticles on Cell Culture Morphology and Photosynthesis (Photosystem II Energy Distribution) in the Green Alga, Chlamydomonas Reinhardtii. *Aquat. Toxicol.* **2010**, *96* (2), 109–114.

(169) Wilson, O. M.; Scott, R. W. J.; Garcia-Martinez, J. C.; Crooks, R. M. Synthesis, Characterization, and Structure-Selective Extraction of 1−3-Nm Diameter AuAg Dendrimer-Encapsulated Bimetallic Nanoparticles. *J. Am. Chem. Soc.* **2005**, *127* (3), 1015–1024.

(170) Shankar, S. S.; Rai, A.; Ahmad, A.; Sastry, M. Rapid Synthesis of Au, Ag, and Bimetallic Au core–Ag Shell Nanoparticles Using Neem (Azadirachta Indica) Leaf Broth. *J. Colloid Interface Sci.* **2004**, *275* (2), 496–502.

(171) Mandal, S.; Selvakannan, P.; Pasricha, R.; Sastry, M. Keggin Ions as UV-Switchable Reducing Agents in the Synthesis of Au Core−Ag Shell Nanoparticles. *J. Am. Chem. Soc.* **2003**, *125* (28), 8440–8441.

(172) Son, S. U.; Jang, Y.; Park, J.; Na, H. B.; Park, H. M.; Yun, H. J.; Lee, J.; Hyeon, T. Designed Synthesis of Atom-Economical Pd/Ni Bimetallic Nanoparticle-Based Catalysts for Sonogashira Coupling Reactions. *J. Am. Chem. Soc.* **2004**, *126* (16), 5026–5027.

(173) Quintanilla, A.; Butselaar-Orthlieb, V. C. L.; Kwakernaak, C.; Sloof, W. G.; Kreutzer, M. T.; Kapteijn, F. Weakly Bound Capping Agents on Gold Nanoparticles in Catalysis: Surface Poison? *J. Catal.* **2010**, *271* (1), 104–114.

(174) Park, J. Y.; Aliaga, C.; Renzas, J. R.; Lee, H.; Somorjai, G. A. The Role of Organic Capping Layers of Platinum Nanoparticles in Catalytic Activity of CO Oxidation. *Catal. Lett.* **2009**, *129* (1–2), 1–6.

(175) Mott, D.; Galkowski, J.; Wang, L.; Luo, J.; Zhong, C.-J. Synthesis of Size-Controlled and Shaped Copper Nanoparticles. *Langmuir* **2007**, *23* (10), 5740–5745.

(176) Effenberger, F. B.; Sulca, M. A.; Machini, M. T.; Couto, R. A.; Kiyohara, P. K.; Machado, G.; Rossi, L. M. Copper Nanoparticles Synthesized by Thermal Decomposition in Liquid Phase: The Influence of Capping Ligands on the Synthesis and Bactericidal Activity. *J. Nanoparticle Res.* **2014**, *16* (11).

(177) Corbierre, M. K.; Cameron, N. S.; Sutton, M.; Laaziri, K.; Lennox, R. B. Gold Nanoparticle/Polymer Nanocomposites: Dispersion of Nanoparticles as a Function of Capping Agent Molecular Weight and Grafting Density. *Langmuir* **2005**, *21* (13), 6063–6072.

(178) Bhattacharya, S.; Srivastava, A.; Pal, A. Modulation of Viscoelastic Properties of Physical Gels by Nanoparticle Doping: Influence of the Nanoparticle Capping Agent. *Angew. Chem.* **2006**, *118* (18), 3000–3003.

(179) Singh, A. K.; Viswanath, V.; Janu, V. C. Synthesis, Effect of Capping Agents, Structural, Optical and Photoluminescence Properties of ZnO Nanoparticles. *J. Lumin.* **2009**, *129* (8), 874–878.

(180) Smetana, A. B.; Klabunde, K. J.; Sorensen, C. M. Synthesis of Spherical Silver Nanoparticles by Digestive Ripening, Stabilization with Various Agents, and Their 3-D and 2-D Superlattice Formation. *J. Colloid Interface Sci.* **2005**, *284* (2), 521–526.

(181) Luo, J.; Han, L.; Kariuki, N. N.; Wang, L.; Mott, D.; Zhong, C. J.; He, T. Synthesis and Characterization of Monolayer-Capped PtVFe Nanoparticles with Controllable Sizes and Composition. *Chem. Mater.* **2005**, *17* (21), 5282–5290.

(182) Xu, Z.; Hou, Y.; Sun, S. Magnetic Core/Shell Fe_3O_4/Au and Fe_3O_4/Au/Ag Nanoparticles with Tunable Plasmonic Properties. *J. Am. Chem. Soc.* **2007**, *129* (28), 8698–8699.

(183) Lu, Y.; Liu, G. L.; Lee, L. P. High-Density Silver Nanoparticle Film with Temperature-Controllable Interparticle Spacing for a Tunable Surface Enhanced Raman Scattering Substrate. *Nano Lett.* **2005**, *5* (1), 5–9.

(184) Wilson, D.; Langell, M. A. XPS Analysis of Oleylamine/Oleic Acid Capped Fe_3O_4 Nanoparticles as a Function of Temperature. *Appl. Surf. Sci.* **2014**, *303*, 6–13.

(185) Wang, Y.; Yang, H. Oleic Acid as the Capping Agent in the Synthesis of Noble Metal Nanoparticles in Imidazolium-Based Ionic Liquids. *Chem. Commun.* **2006**, No. 24, 2545.

(186) Xu, Z.; Shen, C.; Hou, Y.; Gao, H.; Sun, S. Oleylamine as Both Reducing Agent and Stabilizer in a Facile Synthesis of Magnetite Nanoparticles. *Chem. Mater.* **2009**, *21* (9), 1778–1780.

(187) Salzemann, C.; Lisiecki, I.; Urban, J.; Pileni, M.-P. Anisotropic Copper Nanocrystals Synthesized in a Supersaturated Medium: Nanocrystal Growth. *Langmuir* **2004**, *20* (26), 11772–11777.

(188) Xiong, J.; Wang, Y.; Xue, Q.; Wu, X. Synthesis of Highly Stable Dispersions of Nanosized Copper Particles Using L-Ascorbic Acid. *Green Chem.* **2011**, *13* (4), 900.

(189) Yin, M.; Wu, C. K.; Lou, Y.; Burda, C.; Koberstein, J. T.; Zhu, Y.; O'Brien, S. Copper Oxide Nanocrystals. *J. Am. Chem. Soc.* **2005**, *127* (26), 9506–9511.

(190) Lidor-Shalev, O.; Zitoun, D. Reaction Mechanism of "amine–borane Route" towards Sn, Ni, Pd, Pt Nanoparticles. *RSC Adv* **2014**, *4* (109), 63603–63610.

(191) Wei, W.; Lu, Y.; Chen, W.; Chen, S. One-Pot Synthesis, Photoluminescence, and Electrocatalytic Properties of Subnanometer-Sized Copper Clusters. *J. Am. Chem. Soc.* **2011**, *133* (7), 2060–2063.

(192) Schadt, M. J.; Cheung, W.; Luo, J.; Zhong, C.-J. Molecularly Tuned Size Selectivity in Thermal Processing of Gold Nanoparticles. *Chem. Mater.* **2006**, *18* (22), 5147–5149.

(193) Pileni, M. P.; Ninham, B. W.; Gulik-Krzywicki, T.; Tanori, J.; Lisiecki, I.; Filankembo, A. Direct Relationship between Shape and Size of Template and Synthesis of Copper Metal Particles. *Adv. Mater.* **1999**, *11* (16), 1358–1362.

(194) Kawasaki, H.; Kosaka, Y.; Myoujin, Y.; Narushima, T.; Yonezawa, T.; Arakawa, R. Microwave-Assisted Polyol Synthesis of Copper Nanocrystals without Using Additional Protective Agents. *Chem. Commun.* **2011**, *47* (27), 7740.

(195) Zhu, H.; Zhang, C.; Yin, Y. Rapid Synthesis of Copper Nanoparticles by Sodium Hypophosphite Reduction in Ethylene Glycol under Microwave Irradiation. *J. Cryst. Growth* **2004**, *270* (3–4), 722–728.

(196) Wang, H.; Xu, J. Z.; Zhu, J. J.; Chen, H. Y. Preparation of CuO Nanoparticles by Microwave Irradiation. *J. Cryst. Growth* **2002**, *244* (1), 88–94.

(197) Grisaru, H.; Palchik, O.; Gedanken, A.; Palchik, V.; Slifkin, M. A.; Weiss, A. M. Microwave-Assisted Polyol Synthesis of $CuInTe_2$ and $CuInSe_2$ Nanoparticles. *Inorg. Chem.* **2003**, *42* (22), 7148–7155.

(198) Vázquez-Vázquez, C.; Bañobre-López, M.; Mitra, A.; López-Quintela, M. A.; Rivas, J. Synthesis of Small Atomic Copper Clusters in Microemulsions. *Langmuir* **2009**, *25* (14), 8208–8216.

(199) Vilar-Vidal, N.; Blanco, M. C.; López-Quintela, M. A.; Rivas, J.; Serra, C. Electrochemical Synthesis of Very Stable Photoluminescent Copper Clusters †. *J. Phys. Chem. C* **2010**, *114* (38), 15924–15930.

(200) Piccinin, S.; Zafeiratos, S.; Stampfl, C.; Hansen, T. W.; Hävecker, M.; Teschner, D.; Bukhtiyarov, V. I.; Girgsdies, F.; Knop-Gericke, A.; Schlögl, R.; Scheffler, M. Alloy Catalyst in a Reactive Environment: The Example of Ag-Cu Particles for Ethylene Epoxidation. *Phys. Rev. Lett.* **2010**, *104* (3), 035503.

(201) Waugh, K. C.; Hague, M. The Detailed Kinetics and Mechanism of Ethylene Epoxidation on an Oxidised Ag/α-Al_2O_2 Catalyst. *Catal. Today* **2010**, *157* (1), 44–48.

(202) Yue, H.; Zhao, Y.; Ma, X.; Gong, J. Ethylene Glycol: Properties, Synthesis, and Applications. *Chem. Soc. Rev.* **2012**, *41* (11), 4218.

(203) Zoller, U.; Sosis, P. *Handbook of Detergents, Part F: Production*; CRC Press, 2008.

(204) (NIH), N. T. P. (NTP). *Report on Carcinogens (12th Ed.)*; DIANE Publishing, 2011.

(205) P.A. Kilty, N.C. Rol, W.M.H. Sachtler. *Proc 5th Int Congr Catal N.-Holl. Amst.* **1973**, 929.

(206) Grant, R. B.; Lambert, R. M. A Single Crystal Study of the Silver-Catalysed Selective Oxidation and Total Oxidation of Ethylene. *J. Catal.* **1985**, *92* (2), 364–375.

(207) Linic, S.; Barteau, M. A. Formation of a Stable Surface Oxametallacycle That Produces Ethylene Oxide. *J. Am. Chem. Soc.* **2002**, *124* (2), 310–317.

(208) Couves, J.; Atkins, M.; Hague, M.; Sakakini, B. H.; Waugh, K. C. The Activity and Selectivity of Oxygen Atoms Adsorbed on a Ag/α-Al_2O_3 Catalyst in Ethene Epoxidation. *Catal. Lett.* **2005**, *99* (1–2), 45–53.

(209) Atkins, M.; Couves, J.; Hague, M.; Sakakini, B. H.; Waugh, K. C. On the Role of Cs, Cl and Subsurface O in Promoting Selectivity in Ag/α-Al_2O_3 Catalysed Oxidation of Ethene to Ethene Epoxide. *J. Catal.* **2005**, *235* (1), 103–113.

(210) Waugh, K. C.; Hague, M. The Detailed Kinetics and Mechanism of Ethylene Epoxidation on an Oxidised Ag/α-Al_2O_3 Catalyst. *Catal. Today* **2010**, *157* (1), 44–48.

(211) Bukhtiyarov, V. I.; Knop-Gericke, A. Chapter 9 Ethylene Epoxidation over Silver Catalysts. In *Nanostructured Catalysts: Selective Oxidations*; The Royal Society of Chemistry, 2011; pp 214–247.

(212) C. T. Campbell and M. T. Paffett. The role of chlorine promoters in catalytic ethylene epoxidation over the Ag(110) surface. *Appl Surf Sci* **1984**, *19*, 28.

(213) X. E. Verykios, F. P. Stein and R. W. Coughian. Influence of metal crystallite size and morphology on selectivity and activity of ethylene oxidation catalyzed by supported silver *J.Catal* **1980**, *66*, 368.

(214) Cannon, J. C. Ethylene Epoxidation Catalyst. US4235757 A, November 25, 1980.

(215) Minahan, D. M.; Hoflund, G. B. Study of Cs-Promoted, α-Alumina-Supported Silver Ethylene-Epoxidation Catalysts. *J. Catal.* **1996**, *158* (1), 109–115.

(216) Peña, M. A.; Carr, D. M.; Yeung, K. L.; Varma, A. Ethylene Epoxidation in a Catalytic Packed-Bed Membrane Reactor. *Chem. Eng. Sci.* **1998**, *53* (22), 3821–3834.

(217) Lafarga, D.; Al-Juaied, M. A.; Bondy, C. M.; Varma, A. Ethylene Epoxidation on Ag-Cs/α-Al_2O_3 Catalyst: Experimental Results and Strategy for Kinetic Parameter Determination. *Ind. Eng. Chem. Res.* **2000**, *39* (7), 2148–2156.

(218) Linic, S.; Jankowiak, J.; Barteau, M. A. Selectivity Driven Design of Bimetallic Ethylene Epoxidation Catalysts from First Principles. *J. Catal.* **2004**, *224* (2), 489–493.

(219) Linic, S.; Barteau, M. A. Control of Ethylene Epoxidation Selectivity by Surface Oxametallacycles. *J. Am. Chem. Soc.* **2003**, *125* (14), 4034–4035.

(220) Cant, N. W.; Hall, W. K. Catalytic Oxidation: VI. Oxidation of Labeled Olefins over Silver. *J. Catal.* **1978**, *52* (1), 81–94.

(221) Linic, S.; Barteau, M. A. Construction of a Reaction Coordinate and a Microkinetic Model for Ethylene Epoxidation on Silver from DFT Calculations and Surface Science Experiments. *J. Catal.* **2003**, *214* (2), 200–212.

(222) Cowell, J. J.; Santra, A. K.; Lindsay, R.; Lambert, R. M.; Baraldi, A.; Goldoni, A. Bonding and Reactivity of Styrene on Cu(110): Heterogeneous Alkene Epoxidation without the Use of Silver. *Surf. Sci.* **1999**, *437* (1–2), 1–8.

(223) Santra, A. K.; Cowell, J. J.; Lambert, R. M. Ultra-selective Epoxidation of Styrene on Pure Cu{111} and the Effects of Cs Promotion. *Catal. Lett.* **2000**, *67* (2–4), 87–91.

(224) Jankowiak, J. T.; Barteau, M. A. Ethylene Epoxidation over Silver and Copper–silver Bimetallic Catalysts: I. Kinetics and Selectivity. *J. Catal.* **2005**, *236* (2), 366–378.

(225) Monnier, J. R.; Peters, K. T.; Hartley, G. W. The Selective Epoxidation of Conjugated Olefins Containing Allylic Substituents and Epoxidation of Propylene in the Presence of Butadiene. *J. Catal.* **2004**, *225* (2), 374–380.

(226) van Santen, R. A.; de Groot, C. P. M. The Mechanism of Ethylene Epoxidation. *J. Catal.* **1986**, *98* (2), 530–539.

(227) Van Santen, R. A.; Kuipers, H. P. C. E. The Mechanism of Ethylene Epoxidation. In *Advances in Catalysis*; D.D. Eley, H. P. and P. B. W., Ed.; Academic Press, 1987; Vol. Volume 35, pp 265–321.

(228) Reddy, B. M.; Reddy, G. K.; Rao, K. N.; Khan, A.; Ganesh, I. Silica Supported Transition Metal-Based Bimetallic Catalysts for Vapour Phase Selective Hydrogenation of Furfuraldehyde. *J. Mol. Catal. Chem.* **2007**, *265* (1–2), 276–282.

(229) Corma, A.; Iborra, S.; Velty, A. Chemical Routes for the Transformation of Biomass into Chemicals. *Chem. Rev.* **2007**, *107* (6), 2411–2502.

(230) Nagaraja, B. M.; Padmasri, A. H.; David Raju, B.; Rama Rao, K. S. Vapor Phase Selective Hydrogenation of Furfural to Furfuryl Alcohol over Cu–MgO Coprecipitated Catalysts. *J. Mol. Catal. Chem.* **2007**, *265* (1–2), 90–97.

(231) Egeblad, K.; Rass-Hansen, J.; Marsden, C. C.; Taarning, E.; Christensen, C. H. Heterogeneous Catalysis for Production of Value-Added Chemicals from Biomass. *Catalysis* **2009**, *21*, 13–50.

(232) Gowda, A. S.; Parkin, S.; Ladipo, F. T. Hydrogenation and Hydrogenolysis of Furfural and Furfuryl Alcohol Catalyzed by ruthenium(II) Bis(diimine) Complexes. *Appl. Organomet. Chem.* **2012**, *26* (2), 86–93.

(233) Nakagawa, Y.; Nakazawa, H.; Watanabe, H.; Tomishige, K. Total Hydrogenation of Furfural over a Silica-Supported Nickel Catalyst Prepared by the Reduction of a Nickel Nitrate Precursor. *ChemCatChem* **2012**, *4* (11), 1791–1797.

(234) Panagiotopoulou, P.; Vlachos, D. G. Liquid Phase Catalytic Transfer Hydrogenation of Furfural over a Ru/C Catalyst. *Appl. Catal. Gen.* **2014**, *480*, 17–24.

(235) Kijeński, J.; Winiarek, P.; Paryjczak, T.; Lewicki, A.; Mikołajska, A. Platinum Deposited on Monolayer Supports in Selective Hydrogenation of Furfural to Furfuryl Alcohol. *Appl. Catal. Gen.* **2002**, *233* (1–2), 171–182.

(236) Luo, H.; Li, H.; Zhuang, L. Furfural Hydrogenation to Furfuryl Alcohol over a Novel Ni–Co–B Amorphous Alloy Catalyst. *Chem. Lett.* **2001**, *30* (5), 404–405.

(237) Pushkarev, V. V.; Musselwhite, N.; An, K.; Alayoglu, S.; Somorjai, G. A. High Structure Sensitivity of Vapor-Phase Furfural Decarbonylation/Hydrogenation Reaction Network as a Function of Size and Shape of Pt Nanoparticles. *Nano Lett.* **2012**, *12* (10), 5196–5201.

(238) Baker, L. R.; Kennedy, G.; Van Spronsen, M.; Hervier, A.; Cai, X.; Chen, S.; Wang, L.-W.; Somorjai, G. A. Furfuraldehyde Hydrogenation on Titanium Oxide-Supported Platinum Nanoparticles Studied by Sum Frequency Generation Vibrational Spectroscopy: Acid–Base Catalysis Explains the Molecular Origin of Strong Metal–Support Interactions. *J. Am. Chem. Soc.* **2012**, *134* (34), 14208–14216.

(239) An, K.; Musselwhite, N.; Kennedy, G.; Pushkarev, V. V.; Robert Baker, L.; Somorjai, G. A. Preparation of Mesoporous Oxides and Their Support Effects on Pt Nanoparticle Catalysts in Catalytic Hydrogenation of Furfural. *J. Colloid Interface Sci.* **2013**, *392*, 122–128.

(240) Sitthisa, S.; Pham, T.; Prasomsri, T.; Sooknoi, T.; Mallinson, R. G.; Resasco, D. E. Conversion of Furfural and 2-Methylpentanal on Pd/SiO_2 and $Pd–Cu/SiO_2$ Catalysts. *J. Catal.* **2011**, *280* (1), 17–27.

(241) Sitthisa, S.; An, W.; Resasco, D. E. Selective Conversion of Furfural to Methylfuran over Silica-Supported Ni Fe Bimetallic Catalysts. *J. Catal.* **2011**, *284* (1), 90–101.

(242) Tierney, H. L.; Baber, A. E.; Kitchin, J. R.; Sykes, E. C. H. Hydrogen Dissociation and Spillover on Individual Isolated Palladium Atoms. *Phys. Rev. Lett.* **2009**, *103* (24).

(243) Tierney, H. L.; Baber, A. E.; Sykes, E. C. H. Atomic-Scale Imaging and Electronic Structure Determination of Catalytic Sites on Pd/Cu Near Surface Alloys. *J. Phys. Chem. C* **2009**, *113* (17), 7246–7250.

(244) Bellisario, D. O.; Han, J. W.; Tierney, H. L.; Baber, A. E.; Sholl, D. S.; Sykes, E. C. H. Importance of Kinetics in Surface Alloying: A Comparison of the Diffusion Pathways of Pd and Ag Atoms on Cu(111). *J. Phys. Chem. C* **2009**, *113* (29), 12863–12869.

(245) Kyriakou, G.; Boucher, M. B.; Jewell, A. D.; Lewis, E. A.; Lawton, T. J.; Baber, A. E.; Tierney, H. L.; Flytzani-Stephanopoulos, M.; Sykes, Ec. H.; others. Isolated Metal Atom Geometries as a Strategy for Selective Heterogeneous Hydrogenations. *Sci. Wash.* **2012**, *335* (6073), 1209–1212.

(246) Lloyd, S. M.; Lave, L. B.; Matthews, H. S. Life Cycle Benefits of Using Nanotechnology To Stabilize Platinum-Group Metal Particles in Automotive Catalysts. *Environ. Sci. Technol.* **2005**, *39* (5), 1384–1392.

(247) Long, N. V.; Chien, N. D.; Hayakawa, T.; Hirata, H.; Lakshminarayana, G.; Nogami, M. The Synthesis and Characterization of Platinum Nanoparticles: A Method of Controlling the Size and Morphology. *Nanotechnology* **2010**, *21* (3), 035605.

(248) Chen, A.; Zhang, W.; Li, X.; Tan, D.; Han, X.; Bao, X. One-Pot Encapsulation of Pt Nanoparticles into the Mesochannels of SBA-15 and Their Catalytic Dehydrogenation of Methylcyclohexane. *Catal. Lett.* **2007**, *119* (1–2), 159–164.

(249) Li, Z.; He, C. Recent Advances in Silver-Catalyzed Nitrene, Carbene, and Silylene-Transfer Reactions. *Eur. J. Org. Chem.* **2006**, *2006* (19), 4313–4322.

(250) Ukisu, Y.; Miyadera, T.; Abe, A.; Yoshida, K. Infrared Study of Catalytic Reduction of Lean NOx with Alcohols over Alumina-Supported Silver Catalyst. *Catal. Lett.* **1996**, *39* (3–4), 265–267.

(251) Aoyama, N.; Yoshida, K.; Abe, A.; Miyadera, T. Characterization of Highly Active Silver Catalyst for NOx Reduction in Lean-Burning Engine Exhaust. *Catal. Lett.* **1997**, *43* (3–4), 249–253.

(252) Miyadera, T. Selective Reduction of Nitric Oxide with Ethanol over an Alumina-Supported Silver Catalyst. *Appl. Catal. B Environ.* **1997**, *13* (2), 157–165.

(253) Qu, Z.; Cheng, M.; Huang, W.; Bao, X. Formation of Subsurface Oxygen Species and Its High Activity toward CO Oxidation over Silver Catalysts. *J. Catal.* **2005**, *229* (2), 446–458.

(254) Gac, W. The Influence of Silver on the Structural, Redox and Catalytic Properties of the Cryptomelane-Type Manganese Oxides in the Low-Temperature CO Oxidation Reaction. *Appl. Catal. B Environ.* **2007**, *75* (1–2), 107–117.

(255) Hayashi, T.; Uozumi, Y.; Yamazaki, A.; Sawamura, M.; Hamashima, H.; Ito, Y. Silver(I)-Catalyzed Asymmetric Aldol Reaction of Isocyanoacetate. *Tetrahedron Lett.* **1991**, *32* (24), 2799–2802.

(256) Sladojevich, F.; Trabocchi, A.; Guarna, A.; Dixon, D. J. A New Family of Cinchona-Derived Amino Phosphine Precatalysts: Application to the Highly Enantio- and Diastereoselective Silver-Catalyzed Isocyanoacetate Aldol Reaction. *J. Am. Chem. Soc.* **2011**, *133* (6), 1710–1713.

(257) Momiyama, N.; Yamamoto, H. Enantioselective *O* - and *N* -Nitroso Aldol Synthesis of Tin Enolates. Isolation of Three BINAP−Silver Complexes and Their Role in Regio- and Enantioselectivity. *J. Am. Chem. Soc.* **2004**, *126* (17), 5360–5361.

(258) Yamamoto, Y.; Momiyama, N.; Yamamoto, H. Enantioselective Tandem *O* -Nitroso Aldol/Michael Reaction. *J. Am. Chem. Soc.* **2004**, *126* (19), 5962–5963.

(259) Kobayashi, S.; Kakumoto, K.; Mori, Y.; Manabe, K. Chiral Lewis Acid-Catalyzed Enantioselective Michael Reactions in Water. *Isr. J. Chem.* **2001**, *41* (4), 247–250.

(260) Littke, A. F.; Fu, G. C. A Convenient and General Method for Pd-Catalyzed Suzuki Cross-Couplings of Aryl Chlorides and Arylboronic Acids. *Angew. Chem. Int. Ed.* **1998**, *37* (24), 3387–3388.

(261) Wolfe, J. P.; Buchwald, S. L. A Highly Active Catalyst for the Room-Temperature Amination and Suzuki Coupling of Aryl Chlorides. *Angew. Chem. Int. Ed.* **1999**, *38* (16), 2413–2416.

(262) Amatore, C.; Jutand, A. Anionic Pd(0) and Pd(II) Intermediates in Palladium-Catalyzed Heck and Cross-Coupling Reactions. *Acc. Chem. Res.* **2000**, *33* (5), 314–321.

(263) Wolfe, J. P.; Singer, R. A.; Yang, B. H.; Buchwald, S. L. Highly Active Palladium Catalysts for Suzuki Coupling Reactions. *J. Am. Chem. Soc.* **1999**, *121* (41), 9550–9561.

(264) Weck, M.; Jones, C. W. Mizoroki−Heck Coupling Using Immobilized Molecular Precatalysts: Leaching Active Species from Pd Pincers, Entrapped Pd Salts, and Pd NHC Complexes. *Inorg. Chem.* **2007**, *46* (6), 1865–1875.

(265) Polshettiwar, V.; Molnár, Á. Silica-Supported Pd Catalysts for Heck Coupling Reactions. *Tetrahedron* **2007**, *63* (30), 6949–6976.

(266) Lindlar, H.; Dubuis, R. Palladium Catalyst for Partial Reduction of Acetylenes. In *Organic Syntheses*; John Wiley & Sons, Inc., Ed.; John Wiley & Sons, Inc.: Hoboken, NJ, USA, 2003; pp 89–89.

(267) Ghosh, A. K.; Krishnan, K. Chemoselective Catalytic Hydrogenation of Alkenes by Lindlar Catalyst. *Tetrahedron Lett.* **1998**, *39* (9), 947–948.

(268) Rajaram, J.; Narula, A. P. S.; Chawla, H. P. S.; Dev, S. Semihydrogenation of Acetylenes. *Tetrahedron* **1983**, *39* (13), 2315–2322.

(269) Parlett, C. M. A.; Isaacs, M. A.; Beaumont, S. K.; Bingham, L. M.; Hondow, N. S.; Wilson, K.; Lee, A. F. Spatially Orthogonal Chemical Functionalization of a Hierarchical Pore Network for Catalytic Cascade Reactions. *Nat. Mater.* **2015**, *15* (2), 178–182.

(270) Hackett, S. F. J.; Brydson, R. M.; Gass, M. H.; Harvey, I.; Newman, A. D.; Wilson, K.; Lee, A. F. High-Activity, Single-Site Mesoporous Pd/Al_2O_3 Catalysts for Selective Aerobic Oxidation of Allylic Alcohols. *Angew. Chem.* **2007**, *119* (45), 8747–8750.

(271) Lee, A. F.; Ellis, C. V.; Naughton, J. N.; Newton, M. A.; Parlett, C. M. A.; Wilson, K. Reaction-Driven Surface Restructuring and Selectivity Control in Allylic Alcohol Catalytic Aerobic Oxidation over Pd. *J. Am. Chem. Soc.* **2011**, *133* (15), 5724–5727.

(272) Durndell, L. J.; Parlett, C. M. A.; Hondow, N. S.; Isaacs, M. A.; Wilson, K.; Lee, A. F. Selectivity Control in Pt-Catalyzed Cinnamaldehyde Hydrogenation. *Sci. Rep.* **2015**, *5*, 9425.